BNL-220618-2020-JAAM

Polydopamine Surface Coating Synergizes the Antimicrobial Activity of Silver Nanoparticles

I. . Niyonshuti, X. Tong

To be published in "ACS Applied Materials & Interfaces"

August 2020

Center for Functional Nanomaterials

Brookhaven National Laboratory

U.S. Department of Energy

USDOE Office of Science (SC), Basic Energy Sciences (BES) (SC-22)

DISCLAIMER

Polydopamine Surface Coating Synergizes Antimicrobial Activity of Silver Nanoparticles

Isabelle I. Niyonshuti,[1,†] Venkata Rao Krishnamurthi,[2,†] Deborah Okyere,[3] Liang Song,[1] Mourad Benamara,[4] Xiao Tong,[5] Yong Wang,[2,3,6,*] Jingyi Chen[1,3,*]

[1]Department of Chemistry and Biochemistry, University of Arkansas, Fayetteville, AR 72701, USA

[2]Department of Physics, University of Arkansas, Fayetteville, AR 72701, USA

[3]Microelectronics-Photonics Graduate Program, University of Arkansas, Fayetteville, AR 72701, USA

[4]Institute of Nanoscience and Engineering, University of Arkansas, Fayetteville, AR 72701, USA

[5]Center for Functional Nanomaterials, Brookhaven National Laboratory, Upton, NY 11973, USA

[6]Cell and Molecular Biology Graduate Program, University of Arkansas, Fayetteville, AR 72701, USA

[†]These authors contributed to this work equally.

*Corresponding authors: chenj@uark.edu (nanoparticles); yongwang@uark.edu (antimicrobials)

Abstract: Metal nanoparticles especially silver nanoparticles (AgNPs) have drawn increasing attention for antimicrobial applications. Most studies have emphasized on the correlations between the antibacterial potency of AgNPs and the kinetics of metallic to ionic Ag conversion while other antimicrobial mechanisms have been underestimated. In this work, we focused on the surface effects of polydopamine (PDA) coating on the antimicrobial activity of AgNPs. A method of fast deposition of PDA was used to synthesize the PDA-AgNPs with controllable coating thickness ranging from 3 to 25 nm. The antimicrobial activities of the PDA-AgNPs were analyzed by fluorescence-based growth curve assays on *E.coli*. The results indicated that the PDA-AgNPs exhibited significantly higher antibacterial activities than poly(vinylpyrrolidone)-passivated AgNPs (PVP-AgNPs) and PDA themselves. It was found that the PDA coating synergized with the AgNPs to prominently enhance the potency of the PDA-AgNPs against bacteria. The analysis of x-ray photoelectron spectroscopy and Fourier-transform infrared spectroscopy elucidated that the synergistic effects could be originated from the interaction/coordination between Ag and catechol group on the PDA coating. The synergistic effects led to increased generation of reactive oxygen species and the consequent bacterial damage. These findings demonstrated the importance of the surface effects on the antimicrobial properties of AgNPs. The underlying molecular mechanisms shone light on the future development of more potent metal nanoparticle-based antimicrobial agents.

Keywords: PDA, catechol, metal nanoparticles, bacterial growth curve assay, ROS

Introduction

Silver (Ag) has been extensively used as a therapeutic agent in medicine back in ancient history especially for bacterial infections, much earlier than the clinical introduction of antibiotics in 1940s and even earlier than the observation of microorganisms during the late 1700s.[1] Different forms of metallic Ag and Ag compounds including solutions, foils, vessels, and colloids have been demonstrated beneficial in various scenarios from preventing microbial growth in water to combating bacterial infections in surgery. Despite the risk of argyria particularly due to chronic Ag exposure,[2-4] metallic Ag and Ag compounds continue to be widely used in medical devices and health care products in the modern era because the benefit of their antimicrobial effects predominates over the non-life-threatening risk.[1, 5-6] Colloidal Ag nanoparticles (AgNPs) are of particular interest as an active disinfectant that has been incorporated into various matrixes for potential use in different applications.[7-10] For example, incorporation of AgNPs in different textile materials brings to the fabrics not only antimicrobial functions but also beautiful colors due to the optical properties of AgNPs.[8, 11] Embedding AgNPs to the wound dressing can disinfect the wound site and promote tissue repair.[9, 12-13] AgNPs are more active against microbes compared to Ag^+ due to nanoparticle interactions with membrane, protein, and DNA of microorganisms that lead to their exceptional toxicity to the bacterial cells.[14] The size, shape, and surface ligand of AgNPs can influence the antimicrobial activity of the AgNPs,[15-17] and therefore, it is possible to design AgNPs with enhanced antimicrobial properties against infections.

Previous studies have mainly emphasized on the effects of size, shape, and surface ligand on the antimicrobial activity of AgNPs from the oxidation point of view and correlated their antimicrobial activity with the kinetics of Ag(0)→Ag(I) oxidation or Ag(I) ion release.[15, 18-20] However, other mechanisms of AgNPs such as the generation of reactive oxygen species and the

disruption of the biomolecule functions also play significant roles in the antimicrobial actions.[14, 17, 21] Other studies showed that nanoparticles with positively charged surfaces were strong antimicrobial agents.[22-24] In this case, the bacterial response of AgNPs could undergo different pathways highly dependent on their surface characteristics that highlighted the difference in toxicity mechanisms of AgNPs from that of ionic Ag.[22] More recently, we have directly observed that AgNPs increased the fraction of histone-like nucleoid structuring (H-NS) proteins that forms clusters and were able to attach to bacterial cell membrane and undergo a Brownian diffusion.[25] The surfaces of AgNPs passivated by poly(vinylpyrrolidone) (PVP-AgNPs) versus polyethyleneimine (PEI-AgNPs) exhibited different reorganization rate of H-NS proteins. The faster kinetics of H-NS reorganization for PEI-AgNPs appear to be one plausible mechanism responsible for the previously-reported higher antimicrobial activity of PEI-AgNPs compared to PVP-AgNPs.[22]

In this work, we expanded our investigation to the effects of polydopamine (PDA) surface coating on the antimicrobial activity of AgNPs to further our understanding on the role of nanoparticle surface. We choose PDA as the surface coating due to its strong adhesive properties, rich chemical functionalities, and biocompatibility suited for biological applications.[26-27] Numerous reports have shown that deposition/incorporation of AgNPs onto PDA coating could introduce antibacterial properties to the coating on different substrates;[28-54] however, it is unclear whether a PDA surface can synergize the antimicrobial activity of AgNPs and the mechanisms. This study systematically investigated the effects of the degree of dopamine self-polymerization on their antimicrobial activity and correlated them with the physicochemical properties of functionalized AgNPs. Different degree of self-polymerization dopamine was controlled using our previously-established method through the PDA coating time.[55] The morphology and surface

properties of the PDA-coated AgNPs (PDA-AgNPs) were characterized by transmission electron microscopy (TEM), UV-vis spectroscopy, x-ray photoelectron spectroscopy (XPS), and Fourier-transform infrared spectroscopy (FTIR). The antimicrobial activity was evaluated by the bacterial growth curves obtained from our newly-developed method based on fluorescence/optical density assays using a microplate reader.[56] The related biological responses were studied by fluorescence imaging. We observed synergistic effects between the PDA coating and AgNPs, and correlated them with the chemical and biological properties of the PDA-AgNPs to provide a better understanding of nanoparticle surface effects on the antimicrobial activity of AgNPs.

Experimental method

Chemicals and Materials. Silver trifluoroacetate (AgTFA), sodium hydrogen sulfide (NaHS), hydrochloric acid (HCl, 99.999%), and nitric acid (HNO_3, 99.999%) were purchased from Alfa Aesar. Poly(vinylpyrrolidone) (PVP, M.W.=55,000), tris(hydroxymethyl)aminomethane (Trizma base, >99.0%), and dopamine hydrochloride (DA, 99%) were purchased from Sigma Aldrich. Ethylene glycol (EG) was purchased from J.T. Baker. Acetone was purchased from EMD. Unless specified chemicals were used as received and experiments were performed using 18 MΩ H_2O.

Synthesis of PVP-AgNPs. PVP-AgNPs were synthesized by the polyol method.[57] Briefly, 50 mL EG was added to a 250-mL round-bottom flask equipped with a stirring bar and placed in an oil bath at 150 ºC. After the temperature equilibrated (30~45 min), EG solutions of 0.6 mL of 3 mM NaHS, 5 mL of 3 mM HCl, 12.5 mL of 0.25 g PVP, and 4 mL of 282 mM AgTFA were sequentially added to the reaction flask. The reaction was proceeded for additional 75 min. The product was collected by adding acetone to the reaction solution at a ratio of 5:1 and centrifuging at 6,000 rpm for 10 min. The resulting pellet was purified twice with H_2O, collected by centrifugation at 14,000 rpm for 10 min, and resuspended in H_2O for future use.

Synthesis of PDA-coated Ag nanoparticles (PDA-AgNPs). PDA-AgNPs were prepared through self-polymerization of DA on the surface of AgNPs under basic conditions exposed to atmosphere.[55] The reaction was carried out in a 400 mL beaker with a disperser (IKA T 18 digital ULTRA-TURRAX) equipped with a dispersing element (IKA S 18 N-10 G). Initially, 200 mL of water was heated to 50 ºC while dispersed at a speed of 2800 rpm. Trizma base (2 mmol, 0.242 g) was then added to the beaker and allowed to dissolve for 5 min, followed by adding 2 mL of 4.8 nM PVP-AgNPs aqueous suspension into the beaker. After another 5 min, dopamine hydrochloride (5.8 mM, 0.220 g or 1.2 mM, 0.046 g) was added to the beaker to initiate the reaction. The reaction was then allowed to proceed for 5, 15, or 30 min at the dispersing speed of 2800 rpm. At the end, the reaction was quenched by adding 2 mL of 1 vol.% acetic acid and the product was collected by centrifugation at 8,000 rpm for 15 min, purified with water twice, recollected by centrifugation at 14,000 rpm for 10 min at 4 ºC, redispersed in water and stored at 4 ºC for future use. For the control experiments, PDA were prepared the same fashion as PDA-AgNPs but in the absence of AgNPs.

For comparison, dopamine-capped Ag nanoparticles (DA-AgNPs) were prepared by mixing 2 mL of 10 nM (6.0×10^{12} particles/mL) PVP-AgNPs with 20 mL of 1 mM DA solution. The mixture was sonicated for 5 min and then incubated for 24 h at room temperature under magnetic stirring. After incubation, the product was purified with water thrice and collected by centrifugation at 6,500 rpm for 15 min. The nanoparticles were resuspended in H_2O.

Materials Characterization. TEM images were captured using a transmission electron microscope (JEOL JEM-1011) with an accelerating voltage of 100 kV. The hydrodynamic diameters and zeta potentials of the products were measured using a dynamic light scattering (DLS) instrument (Brookhaven ZetaPALS). The concentration of Ag was determined using an

inductively coupled plasma mass spectrometer (Thermo Scientific iCAP Q ICP-MS). UV-vis spectra were taken on a UV-vis spectrophotometer (Agilent Cary 50). XPS experiments were carried out in an ultrahigh vacuum (UHV) system with base pressures < 5 x 10^{-9} Torr equipped with a hemispherical electron energy analyzer (SPECS, PHOIBOS 100) and twin anode x-ray source (SPECS, XR50). Al K_α (1486.6 eV) radiation was used at 15 kV and 20 mA. The angle between the analyzer and x-ray source is 45^o and photoelectrons were collected along the sample surface normal. The XPS spectra was analyzed using CasaXPS. The FTIR spectra were obtained on an FTIR Spectrometer (Shimadzu IRAffinity-1S) using a KBr pellet method.

Antimicrobial Evaluation. An *E. coli* K-12 strain (MG1655) transformed with a plasmid encoding enhanced green fluorescent proteins (EGFP) and ampicillin resistance was used in this study. The bacteria were grown at 37 °C overnight in 6 mL of Luria Broth (LB) medium supplemented with ampicillin in a shaking incubator with orbital rotation at 250 rpm. On the second day, the overnight culture was diluted in 40 mL of fresh LB medium to reach OD_{600} = 0.05. Nanoparticle suspensions were added to the fresh culture aliquots (1 mL) to reach final concentrations of 0 (negative control; without nanoparticles), 20, 40, 60, and 80 μg/mL.

For the growth-curve assay with a microplate reader, 96-well clear bottom microplates were sterilized by incubating the wells with 200 proof ethanol for 5 min and then exposing the empty wells to UV light at 254 nm for 15 min. To avoid water condensation on the microplate lids during the measurements, the lids were coated with Triton X-100.[58] Briefly, 4 mL of 0.05% Triton X-100 in 20% ethanol was added to each microplate lid and incubated at room temperature for 15 s, followed by pouring off the Triton solution. The microplates were then air dried before use.

To measure the growth of bacteria, 200 μL of the bacterial cultures (with or without nanoparticles) were transferred to the microplate wells. The microplates were covered with the

pre-processed lids and placed in a microplate reader (BioTek Synergy H1 Hybrid) to monitor both the fluorescence (excitation = 488 nm; emission = 525 nm) and the optical density (OD) at 600 nm of the bacteria in the wells. Wells with 200 µL LB medium supplemented with ampicillin were used as blanks. The plates were maintained at 37°C and rotated at 355 rpm. The fluorescence and OD readings were acquired every 10 min for 48 h. Each sample was measured with 4 – 6 replicates. The time series of the fluorescence-based growth curves for each sample were obtained by subtracting the mean of the fluorescence of the blanks at each time point from the mean of the fluorescence of the sample. In contrast, the time series of the OD-based growth curves for each sample were obtained by subtracting both the mean of the OD of the blanks at each time point and the initial OD (i.e., at time t = 0) from the mean of the OD values, in order to partly remove the contribution of AgNPs to the OD values.[59] The fluorescence-based growth curves were analyzed using our recently developed method based on the time derivatives.[56] Briefly, the fluorescence-based growth curves were first smoothed (with a Hann window with a size of 15), followed by calculating the derivatives numerically, $\left.\frac{\Delta \mathrm{F}}{\Delta \mathrm{t}}\right|_i = \frac{F_{i+1}-F_i}{\Delta t}$, and $\left.\frac{\Delta^2 F}{\Delta t^2}\right|_i = \frac{\left.\frac{\Delta \mathrm{F}}{\Delta \mathrm{t}}\right|_{i+1} - \left.\frac{\Delta \mathrm{F}}{\Delta \mathrm{t}}\right|_i}{\Delta t}$, where F is the fluorescence intensity and $\Delta t = 0.167$ h is the time interval between adjacent fluorescence readings. From the peaks in the second-order time derivatives, $\Delta^2\mathrm{F}/\Delta\mathrm{t}^2$, we determined the peak locations (τ_p^f) and peak heights (η_p^f).

CellROX® Staining and Quantification. The bacteria were grown at 37°C overnight in 7 mL of LB medium in a shaking incubator with orbital rotation at 250 rpm. On the second day, the overnight culture was diluted in 7 mL of fresh LB medium so that OD_{600} = 0.05. The fresh culture was regrown at 37ºC with orbital rotation at 250 rpm to reach OD_{600} = 0.3. The culture was aliquoted to 1 mL aliquots, followed by addition of PDA15-AgNPs, PDA15, or PVP-AgNPs to reach a final concentration of 60 µg/mL. Untreated bacteria were used as a negative control. After

incubating the samples at 37ºC and 250 rpm for 2 hours, CellROX® Orange Reagent (Thermo Fisher Scientific, Waltham, MA) was added to the untreated and treated bacteria at a final concentration of 5 μM and incubated at 37ºC with orbital shaking at 250 rpm for 30 min. The bacteria were harvested by centrifugation at 1000 g for 10 min, followed by resuspension in 1 mL 1× PBS. The collected bacteria were further washed by centrifugation and resuspension in 1× PBS for five times to remove media and dyes. The stained bacteria were transferred to 5×5 mm agarose pads (3% in 1× PBS). The agarose pad with the stained bacteria were flipped onto a clean coverslip (cleaned with sonication in detergent, 1 M NaOH, 100% ethanol, and ultra-pure water sequentially). Chambers were then constructed by sandwiching rubber O-rings between the coverslips and clean microscope slides. The chambers were sealed using epoxy glue and then mounted on a microscope (with a 100× objective) for fluorescence imaging (excitation at 532 nm) and brightfield imaging. The fluorescence intensities of 100 bacteria for each sample were quantified using ImageJ.[60-62]

MitoTracker Staining and Quantification. Bacterial samples (1 mL each) were prepared using a similar procedure as that for the CellROX® staining experiments. Instead of the CellROX® staining reagent, MitoTracker Green FM dye (Thermo Fisher Scientific, Waltham, MA) was added to the untreated and treated bacteria at a final concentration of 300 nM and incubated at room temperature with orbital shaking at 250 rpm for 30 min. The stained bacteria were transferred to agarose pads, followed by fluorescence imaging (excitation at 488 nm) and brightfield imaging. The fluorescence intensities of 140 bacteria for each sample were quantified using ImageJ.[60-62]

Propidium Iodide (PI) Staining and Quantification. Bacterial samples (1 mL each) were prepared similarly to those in the MitoTracker staining experiments except that the bacteria were fixed with 3.8% formaldehyde (Sigma-Aldrich, St. Louis, MO) before adding PI staining dyes (G-

Biosciences, St. Louis, MO). After incubating the samples at room temperature with light shielded for 20 min, the bacteria were mounted on agarose pads, followed by phase contrast imaging and fluorescent imaging (excitation at 532 nm, with a 40× objective). The percentage of PI-stained bacterial cells were quantified using ImageJ.[60-62]

Scanning Electron Microscopy (SEM) and Fluorescent Imaging of Nanoparticle-Treated Bacteria. The nanoparticle-treated and fixed bacterial samples (1 mL each) were prepared similarly to those in the PI staining experiments. For SEM imaging, the bacteria were harvested by centrifugation at 1000 g for 10 min, followed by resuspension in 1 mL autoclaved water. The collected bacteria were further washed by centrifugation and resuspension in water for three times to removal salts from the samples. The prepared bacteria in water (1 mL) were dropped on silicon substrates and dried at room temperature for SEM imaging on FEI Nova Nanolab 200 using 15 kV acceleration voltage and 5 mm working distance. For fluorescent imaging, the bacteria were harvested by centrifugation at 1000 g for 10 min, followed by resuspension in 1 mL PBS. The prepared bacteria were mounted on agarose pads, followed by fluorescent imaging (excitation at 532 nm, with a 100× objective).

Results and Discussion

To test the hypothesis of synergistic antimicrobial effects, we deposited the PDA coating on the surface of PVP-AgNPs with different lengths of coating time that was indicated in the abbreviations, PDA5-AgNPs, PDA15-AgNPs, and PDA30-AgNPs, for 5, 15, and 30 min, respectively, as illustrated in Figure 1A. Figure 1, B-E, shows the TEM images of the PVP-AgNPs and PDA-AgNPs with different coating time. After the PDA coating process, the average size of the nanoparticles measured from TEM images increased from 32 nm for PVP-AgNPs to 36, 43, and 54 nm for PDA5-AgNPs, PDA15-AgNPs, and PDA30-AgNPs, respectively. By taking the

difference between PDA-AgNPs and PVP-AgNPs, the PDA coating thickness was estimated to be 4 to 11, and 22 nm and increased with the deposition time from 5 to 15, and 30 min. The deposition rate and coating thickness were consistent with our previously-established reaction kinetics of PDA coating process.[55] The coating kinetics was drastically slowed down when the reaction was performed in water overnight as dopamine-functionalized AgNPs (DA-AgNPs). The coating thickness was estimated to be 4 nm from the TEM image in Figure S1A. The hydrodynamic diameters and zeta potentials of different nanoparticles were listed in Table S1. The hydrodynamic diameters of PDA15-AgNPs and PDA30-AgNPs are on the order of 200 nm, larger than those of PVP-AgNPs, PDA5-AgNPs, and DA-AgNPs which are on the order of 100 nm. The zeta potentials of AgNPs surface coated with PDA, PVP, or DA in PBS at pH 7.4 are all negative values, on the order of -10 mV, indicating that these AgNPs are negatively charged. For comparison, the PDA samples, PDA5, PDA15, and PDA30, were also synthesized under the same reaction conditions but the absence of AgNPs. They appeared to be spherical nanoparticles in the TEM images with the sizes of 29, 38, and 45 nm for PDA5, PDA15, and PDA30, respectively, as shown in Figure S1, B-D.

The increase of the coating thickness as a function of time was also verified by the UV-vis and XPS spectroscopy. Figure 2A displays the normalized UV-vis spectra obtained from the aqueous suspensions of PVP-AgNPs, PDA5-AgNPs, PDA15-AgNPs, and PDA30-AgNPs. The zoom-in spectra indicated the localized surface plasmon resonance (LSPR) of AgNPs shifted to the longer wavelength as the coating thickness increased (Figure 2B). The LSPR peak shifted from 420 nm for PVP-AgNPs to 435, 442, and 450 nm for PDA5-AgNPs, PDA15-AgNPs, and PDA30-AgNPs, respectively, following the same trend as our previously-established relationship between LSPR shift and PDA coating thickness.[55] Similarly, the LSPR peak became broader due to the

inhomogeneity of the coating thickness as it can be seen in the TEM images. The increase of the PDA coating thickness was also confirmed by quantitative analysis of N to Ag ratio from XPS as shown in Figure 2C. Since the experimental conditions were the same for all the sample measurements, we can assume that the analysis depth is the same across different samples. The typical probing depth of XPS is less than 10 nm from the surface well below the size of the nanoparticle and thus the analysis indeed reflects the composition of the nanoparticle surface. Because the monomers of PVP (N-vinylpyrrolidone) and PDA (dopamine) contain only one N atom, the increase of N to Ag ratio from 0.40 for PVP-AgNPs to 1.59, 2.90 and 7.57 for PDA5-AgNPs, PDA15-AgNPs PDA30-AgNPs suggests the PDA coating became thicker with the increased PDA deposition time.

We then evaluate the antimicrobial activities of these PDA-AgNPs with different coating time (PDA5-AgNPs, PDA15-AgNPs, and PDA30-AgNPs) against *E.coli* and compared the results of the control PVP-AgNPs. In this study, an *E. coli* K-12 strain (MG1655) transformed with a plasmid encoding enhanced green fluorescent proteins (EGFP) and ampicillin resistance was used. We incubated the same concentration of bacterial suspension that has an OD_{600} reading of 0.05 with different concentrations of nanoparticles from 0 to 20, 40, 60, and 80 μg/mL (referred to the concentration of Ag) and monitored the fluorescence of the bacteria (excitation = 488 nm; emission = 525 nm) using a microplate reader. Note that the commonly used OD measurements were not chosen in this study due to interferences of the AgNPs' contribution to the OD at 600 nm. The fluorescence-based bacterial growth curves were shown as functions of time in Figure 3. Compared to the PVP-AgNPs (Figure 3A), the PDA coating significantly improved the antimicrobial effects of AgNPs (Figure 3, B-D). At the concentration of 60 μg/mL and above, the PDA-AgNPs completely suppressed the bacterial growth. The increased antimicrobial activity

follows the order of PDA15-AgNPs ≈ PDA30-AgNPs > PDA5-AgNPs > PVP-AgNPs.

To investigate the role of the PDA coating to the antimicrobial effects of the AgNPs, we evaluated the antimicrobial activities of PDA themselves synthesized at the same conditions as the coating process but in absence of AgNPs. Figure 4 shows the bacterial growth plots of DA monomer and PDA nanoparticles after 5, 15, and 30 min reactions as abbreviated PDA5, PDA15, and PDA30. As it can be seen, all of them display some degrees of bacterial inhibition effects, but none of them can completely suppress the bacterial after 48 h incubation up to 80 μg/mL. PDA15 and PDA30 overall shows a better bacterial inhibition agent than DA and PDA5. This observation appears to correlate well with that observed for the PDA-AgNPs, that is, PDA15-AgNPs and PDA30-AgNPs having better antimicrobial properties than PDA5-AgNPs. In other words, PDA coating plays a significant role to enhance the antimicrobial properties of AgNPs.

We further determine whether such enhancement from the PDA coating is simply an additive effect or a more-interesting synergetic effect to the antimicrobial properties of AgNPs, by the new method that we developed recently.[56] In this method, the second-order time derivative of the fluorescence growth curve (F) is taken ($\Delta^2F/\Delta t^2$), showing a bell-shaped peak. The peak location (τ_p^f) and height (η_p^f) are related to the lag time and growth rate of the bacteria, as well as the expression rate, maturation rate, and degradation rate of GFP proteins; therefore, changes in the peak location and height are able to report changes in the growth behavior of the bacteria.

Figure 5 plots the peak location and height extracted from the fluorescence growth curves in Figure 3 and 4. We observed that all the samples decreased the peak height (η_p^f, Figure 5A). PDA15-AgNPs and PDA30-AgNPs exhibited the strongest effects while DA showed the least, consistent with the qualitative observations from the fluorescence growth curves (Figure 3 and 4). Note that if the fluorescence growth curves were too shallow (e.g., curves for PDA15-AgNPs and

PDA30-AgNPs at ≥40 μg/mL, Figure 3C and 3D), peaks were not identified reliably and thus the peak heights (or locations) were not shown. Interestingly, we observed that DA and PDA did not change the peak location (τ_p^f) of the time derivative of fluorescence growth curves ($\Delta^2F/\Delta t^2$), while τ_p^f increased significantly (i.e., the peak shifted to longer times) as the concentration of PVP-AgNPs or PDA-AgNPs increased. Furthermore, the changes of τ_p^f in the presence of the PDA-AgNPs were larger than that due to PVP-AgNPs. This observation is significant because it suggests that the PDA coating synergizes the antimicrobial activity of AgNPs, which could be seen from the changes in the peak locations.

We further take the concentration of 20 μg/mL as an example to elucidate the synergistic effects observed from the PDA-AgNPs. Compared to the control (i.e., 0 μg/mL), the changes of the peak location due to PDA at 20 μg/mL (i.e., PDA5, PDA15, and PDA30) were $\delta\tau_{PDA} = 0$, while that for AgNPs without PDA (i.e., PVP-AgNPs) at the same concentration was $\delta\tau_{AgNP} \approx$ 0.2 hr. However, the changes due to PDA-AgNPs at the same concentration, $\delta\tau_{PDA-AgNP}$, ranging from 3.3 h (PDA5-AgNPs) to 4.7 h (PDA30-AgNPs), showed that $\delta\tau_{PDA-AgNP} \gg \delta\tau_{PDA} + \delta\tau_{AgNP}$. In other words, in terms of the shift of peak locations of the time derivatives of the fluorescence growth curves, the effect of PDA-AgNPs was much larger than sum of the effects from PDA and AgNPs. Therefore, the enhancement in the antimicrobial activities of AgNPs due to the PDA coating is not additive but synergetic.

To further confirm the synergistic effects of the PDA coating and AgNPs, we also examined the OD growth curves of the same samples (Figure S2), which suffered from multiple scattering[63] at high OD values and interference from the contributions of the AgNPs to the optical density at 600 nm. The first problem of multiple scattering could be partly avoided by focusing on low OD values (e.g., < 1.0), while the second problem was much more complicated. Nonetheless, it was

possible to compare qualitatively among the different samples if we vertically shifted the growth curves by subtracting the initial OD value from each growth curve, $OD_{600}(t) = OD_{600}^{raw}(t) - OD_{600}^{raw}(0)$.[59] We observed that the growth curves of the bacteria treated with PDA5, PDA15, or PDA30 overlapped with the untreated control, indicating that PDA alone did not change the growth behavior of the bacteria. PVP-AgNPs shifted the growth curve to the right by several hours, indicating an elongation of the lag time and consistent with our previous observations qualitatively.[59] It is noted that the OD measurements using the microplate reader showed a peak around 1-2 h for the bacteria treated with PVP-AgNPs, which was also present, but much less dominant in cuvette-based growth curve measurements, presumably due to the interactions of the AgNPs with the medium (e.g., precipitation and re-dissolution of AgNPs in Cl^--rich solutions) and/or the bacteria (e.g., adsorption of AgNPs to the bacterial surfaces). In contrast, PDA-AgNPs suppressed the growth of bacteria for at least 24 hours. The elongation of the lag time in the presence of PDA-AgNPs was again much longer than the sum of those due to PDA or AgNPs alone, providing evidence to support the conclusion that PDA coating synergizes the antimicrobial activities of AgNPs.

To understand the synergistic effect between the PDA coating and AgNPs, we looked into the chemical properties of the PDA-AgNPs. Figure 6A displays the XPS spectra of Ag 3d of the PDA-AgNPs with the comparison of PVP-AgNPs with a 6 eV energy splitting between Ag 3d5/2 and Ag 3d3/2. The binding energy (BE) of Ag 3d5/2 shifted from 366.8 eV for PVP-AgNPs to 367.7, 367.8, and 367.4 eV for PDA5-AgNPs, PDA15-AgNPs, and PDA30-AgNPs, respectively. The approximately 1 eV upward shift of Ag 3d on the surface of AgNPs with the PDA coating suggests that compared to PVP-AgNPs, PDA-AgNPs could be attributed to a decrease of initial-state effect due to chemical environment change or a loss of electrons from Ag. From the valence point of

view, the higher valence/oxidation state could increase the antimicrobial potency of Ag;[64] however, the coordination between Ag and PDA through mainly the catechol group may play an important role in governing the antimicrobial activity of the PDA-AgNPs.[65] The presence of the catechol group/partially oxidized catechol group was evidenced by the XPS analysis of oxygen. From the O 1s spectra in Figure 6B, an approximately 0.5 eV upward shift of the O 1s BE was observed from 531.4 eV for PVP-AgNPs to 532.1, 532.1, and 531.9 eV for PDA5-AgNPs, PDA15-AgNPs, and PDA30-AgNPs, respectively. The typical BE of O 1s for organic compounds can be assigned as follows: from 531.3 to 532.0 eV for N-C=O and from 532.7 to 533.1 eV for C-OH (aliphatic), as well as 532.2 for C=O (aromatic) and 533.6 eV for C-OH (aromatic).[66] The deconvoluted spectra of O 1s in Figure S3 indicates the increase of the hydroxyl percentage from ~10% to ~25% before and after PDA coating.

The increased hydroxyl context after PDA coating was also confirmed by the indirect evidence from the analysis of FTIR spectra of DA, PDA, and PDA-AgNPs, as shown in Figure 7. The FTIR spectrum of monomer DA exhibited a number of characteristic peaks that can be assigned to the N-H stretching (3370 cm^{-1}) and bending (1614 cm^{-1}) vibrations of the primary amine, the intermolecular hydrogen bonded O-H stretching (3250 cm^{-1}) of the catechol, the aromatic ring stretch (1600, 1496, and 1469 cm^{-1}), and the aromatic C-H stretch (3036 cm^{-1}) and methyl C-H stretch (2041 cm^{-1}).[67-68] Exposure of DA to air under basic condition (tris-base, pH 8.5) leads to oxidation of DA to dopamine quinone and cyclic reaction to 5,6-dihydroxyindole and its oxidized form indole-5,6-quinone (Figure 1A). These cyclic and oxidized monomers further react to form PDA with increased structural complexity. All the PDA spectra exhibited a board band at ~3420 cm^{-1} that can be assigned to intermolecular hydrogen bonded O-H stretch with the N-H stretch of secondary amine buried underneath, and a set of distinguishable bands at 1632, 1455, and 1160

cm^{-1} that can be attributed to the aromatic ring stretching vibrations of the polyindole structures.[69] Additionally, the band at 1730 cm^{-1} corresponding to C=O stretching vibration[67-68] appeared at the PDA spectra; however, the relative intensity of C=O stretch to the polyindole ring stretch decrease with increased reaction time. Similar trend was observed on the PDA-AgNPs meaning that the ratio of 5,6-dihydroxyindole to indole-5,6-quinone increased as the PDA coating became thicker. This observation suggests that the polymerization of the monomers can lead to the conversion of quinone back to catechol agreed with the theoretical predictions;[70] however, the further extension of the exposure of PDA to O_2 would eventually convert catechol to quinone.

Although the FTIR is a bulk technique, it only probes the polymer structures. Since the polymer is the coating layer on the nanoparticles with its thickness increasing from 4 for PDA5-AgNP to 11 and 22 nm for PDA15-AgNP and PDA30-Ag, respectively, XPS and FTIR, in this case, probe mostly the surface (i.e. coating layer) of the nanoparticles. From the quantitative analysis of XPS, we observed that Ag-to-polymer ratio decreased with increasing coating thickness (Figure 2C). The observed Ag signals in the thicker polymer coating (>10 nm), well above the probing depth of XPS, suggest that Ag is present in the polymer coating. The FTIR results indicate the presence of catechol group in the polymer coating of the PDA-AgNP nanoparticles (Figure 7B) which agree with the XPS findings (Figure S3). The interaction between the Ag in the polymer coating and the O of the catechol group can be seen based on the shifts of Ag 3d and O 1s in the XPS spectra (Figure 6) that the O donates electrons to the Ag, suggesting the plausible coordination between Ag and the catechol group of the PDA coating. Such metal-catechol coordination can lead to the synergistic effect of the PDA-AgNPs as a potent antimicrobial agent because heavy metals such as the Ag^0/Ag ions from the AgNPs can catalyze the redox cycling of catechol group in the PDA coating.[65] As a result, an electron from the catechol-quinone redox cycle can convert molecular

oxygen (O_2) to superoxide (O_2^-), which can be further reduced to hydrogen peroxide (H_2O_2) and hydroxyl radicals (·OH) in the presence of heavy metals such as Ag. We used CellROX® Orange Reagent to quantify the ROS of PDA15-AgNP treated cells compared to those of the control (cells with no treatment), PDA15-treated cells, and PVP-AgNP treated cells (Figure 8A, with treatment time of 2 h). Despite large cell-to-cell variations, quantitative analysis of fluorescence signals indicates a 50% enhancement, on average, in the intensities of the PDA15-AgNP treated cells compared to the others (Figure 8B).

It is known that ROS can cause oxidative damages of cell membranes.[71] The biological effects of PDA-AgNPs to the bacterial cell membrane were examined by MitoTracker Green FM dye and PI dye after treating the bacterial cells with PDA15-AgNPs, PDA15, and PVP-AgNPs for 2 h. The attachment of the nanoparticles on the bacteria was investigated by both fluorescent imaging and SEM imaging. The fluorescent images of nanoparticles showed that more aggregated PDA-AgNPs were around and/or attached to the bacteria than PDA and PVP-AgNPs (Figure S4A), which agreed with the SEM results (Figure S4B). By staining the bacterial membrane using MitoTracker Green FM dye, we observed that the bacterial membrane became brighter after subjecting the bacteria to PDA15-AgNPs (Figure 9A), indicating the change of bacterial membrane potential. To quantify this effect, we estimated the mean intensities of 140 bacteria for each sample (i.e., control – untreated, treated with PDA15-AgNP, PDA15, and PVP-AgNP, respectively) and observed that, although increased brightness was observed for all the treated bacteria, those treated with PDA15-AgNPs showed the highest intensity increase (Figure 9B). In addition, to assess the significance of membrane damage caused by the nanoparticle, we stained the bacterial DNA with PI. The rationale is that if PI molecules could enter the bacteria to stain DNA, the membrane damage is significant enough to allow influx of ions and other small organic molecules. Representative

images of untreated and treated bacteria are shown in Figure 9C, where the fluorescent images from PI staining (purple) are superposed on the phase contrast images (grayscale). It was observed that, compared to the control, more than four-fold of the bacteria treated with PDA15-AgNPs were stained by PI (Figure 9D), suggesting that PDA-AgNPs caused more membrane damage compared to PVP-AgNPs. In contrast, the bacteria treated by PDA15 alone showed much lower percentage of PI-stained bacteria (slightly higher than the control though), indicating that PDA alone did not cause significant membrane damage. These results confirmed that the synergistic effects of PDA-AgNPs led to greater antimicrobial activity than the simple addition of PDA and AgNPs.

Conclusion

We have synthesized the PDA-AgNPs with controllable PDA coating thickness to study the surface effects on the antimicrobial activity of AgNPs. The thickness of the PDA coating on the AgNPs increased with the PDA deposition time from 3.5 to 11.4, and 22.1 nm for the reaction time of 5, 15, and 30 min. The antimicrobial activities of the PDA-AgNPs were evaluated by the fluorescence-based growth curve assays on *E.coli*, indicating that PDA-AgNPs were better antimicrobial agents than PVP-AgNPs and PDA themselves. More importantly, the synergistic effects between the PDA coating and the AgNPs were found to significantly increase the potency of AgNPs against *E.coli*. XPS and FTIR analysis unveiled the coordination between Ag and catechol group on the PDA coating that could be responsible for the synergistic effects. The PDA-Ag interaction of PDA-AgNPs increased the ROS generation and caused significant damage to the bacterial membrane. The result indicated that catechol-rich PDA coating exhibited more pronounced synergistic effects on the antimicrobial of AgNPs. Our findings also elucidated the molecular mechanism for the previous studies which illustrated the importance of the choice of fabrication methods in yielding a PDA surface with strong antimicrobial properties.[72-73] This study

not only demonstrated the importance of the surface effects on the antimicrobial properties of AgNPs, but also laid out guiding principles for the future development of metal nanoparticle-based antimicrobial agents.

SUPPORTING INFORMATION

Table of hydrodynamic diameter and zeta potential measurements of surface-modified AgNPs; TEM images of the PDA samples; bacterial growth curves using OD measurement; XPS deconvoluted spectra of O 1s of the PDA-AgNPs samples; and fluorescence and SEM images of bacteria treated with different conditions.

ACKNOWLEDGEMENT

This work was supported in part by the grant from National Science Foundation NSF CBET 1826642 and by the Center for Advanced Surface Engineering from NSF EPSCoR OIA 1457888. ICP-MS measurements were carried out at the Arkansas Mass Spectrometry facility, which is supported by the Arkansas Biosciences Institute. XPS measurements were performed at the Center for Functional Nanomaterials (CFN), which is a U.S. DOE Office of Science Facility, at BNL under Contract No. DE-SC0012704.

References

1. Alexander, J. W., History of the Medical Use of Silver. *Surg. Infect.* **2009**, *10*, 289-292.
2. Hill, W. R.; Pillsbury, D. M., *Argyria: The Pharmacology of Silver*; Williams & Wilkins, 1939.
3. Bracey, N. A.; Zipursky, J. S.; Juurlink, D. N., Argyria Caused by Chronic Ingestion of Silver. *CMAJ* **2018**, *190*, E139-E139.
4. Ferrara, G.; Filosa, A.; Mariani, M. P.; Fasanella, L., Occupational Argyria of the Nasal Mucosa. *Head Neck Pathol.* **2018**, *12*, 252-254.
5. Lansdown, A. B., Silver in Health Care: Antimicrobial Effects and Safety in Use. In *Biofunctional Textiles and the Skin*, Karger Publishers: 2006; Vol. 33, pp 17-34.
6. Marambio-Jones, C.; Hoek, E. M., A Review of the Antibacterial Effects of Silver Nanomaterials and Potential Implications for Human Health and the Environment. *J. Nanopart. Res.* **2010**, *12*, 1531-1551.
7. Rai, M.; Yadav, A.; Gade, A., Silver Nanoparticles as a New Generation of Antimicrobials. *Biotech. Adv.* **2009**, *27*, 76-83.
8. Shahid ul, I.; Butola, B. S.; Mohammad, F., Silver Nanomaterials as Future Colorants and Potential Antimicrobial Agents for Natural and Synthetic Textile Materials. *RSC Adv.* **2016**, *6*, 44232-44247.
9. Kalantari, K.; Mostafavi, E.; Afifi, A. M.; Izadiyan, Z.; Jahangirian, H.; Rafiee-Moghaddam, R.; Webster, T. J., Wound Dressings Functionalized with Silver Nanoparticles: Promises and Pitfalls. *Nanoscale* **2020**, *12*, 2268-2291.
10. Deshmukh, S. P.; Patil, S. M.; Mullani, S. B.; Delekar, S. D., Silver Nanoparticles as an Effective Disinfectant: A Review. *Mater. Sci. Eng. C* **2019**, *97*, 954-965.
11. Simončič, B.; Klemenčič, D., Preparation and Performance of Silver as an Antimicrobial Agent for Textiles: A Review. *Text. Res. J.* **2016**, *86*, 210-223.
12. Boateng, J.; Catanzano, O., Silver and Silver Nanoparticle-Based Antimicrobial Dressings. *Therapeutic Dressings and Wound Healing Applications* **2020**, 157-184.
13. Ogunsona, E. O.; Muthuraj, R.; Ojogbo, E.; Valerio, O.; Mekonnen, T. H., Engineered Nanomaterials for Antimicrobial Applications: A Review. *Appl. Mater. Today* **2020**, *18*, 100473.
14. Durán, N.; Durán, M.; de Jesus, M. B.; Seabra, A. B.; Fávaro, W. J.; Nakazato, G., Silver Nanoparticles: A New View on Mechanistic Aspects on Antimicrobial Activity. *Nanomedicine* **2016**, *12*, 789-799.
15. Stabryla, L. M.; Johnston, K. A.; Millstone, J. E.; Gilbertson, L. M., Emerging Investigator Series: It's Not All About the Ion: Support for Particle-Specific Contributions to Silver Nanoparticle Antimicrobial Activity. *Environ. Sci. Nano* **2018**, *5*, 2047-2068.
16. Zheng, K.; Setyawati, M. I.; Leong, D. T.; Xie, J., Antimicrobial Silver Nanomaterials. *Coord. Chem. Rev.* **2018**, *357*, 1-17.
17. Gharpure, S.; Akash, A.; Ankamwar, B., A Review on Antimicrobial Properties of Metal Nanoparticles. *J. Nanosci. Nanotech.* **2020**, *20*, 3303-3339.
18. Helmlinger, J.; Sengstock, C.; Groß-Heitfeld, C.; Mayer, C.; Schildhauer, T. A.; Köller, M.; Epple, M., Silver Nanoparticles with Different Size and Shape: Equal Cytotoxicity, but Different Antibacterial Effects. *RSC Adv.* **2016**, *6*, 18490-18501.
19. Le Ouay, B.; Stellacci, F., Antibacterial Activity of Silver Nanoparticles: A Surface Science Insight. *Nano Today* **2015**, *10*, 339-354.

20. Kubo, A.-L.; Capjak, I.; Vrček, I. V.; Bondarenko, O. M.; Kurvet, I.; Vija, H.; Ivask, A.; Kasemets, K.; Kahru, A., Antimicrobial Potency of Differently Coated 10 and 50 nm Silver Nanoparticles against Clinically Relevant Bacteria *Escherichia Coli* and *Staphylococcus Aureus*. *Colloids Surf. B* **2018**, *170*, 401-410.
21. Reidy, B.; Haase, A.; Luch, A.; Dawson, K. A.; Lynch, I., Mechanisms of Silver Nanoparticle Release, Transformation and Toxicity: A Critical Review of Current Knowledge and Recommendations for Future Studies and Applications. *Materials* **2013**, *6*, 2295-2350.
22. Ivask, A.; ElBadawy, A.; Kaweeteerawat, C.; Boren, D.; Fischer, H.; Ji, Z.; Chang, C.H.; Liu, R.; Tolaymat, T.; Telesca, D., et al., Toxicity Mechanisms in *Escherichia Coli* Vary for Silver Nanoparticles and Differ from Ionic Silver. *ACS Nano* **2014**, *8*, 374-386.
23. Chang, T. Y.; Chen, C. C.; Cheng, K. M.; Chin, C. Y.; Chen, Y. H.; Chen, X. A.; Sun, J. R.; Young, J. J.; Chiueh, T. S., Trimethyl Chitosan-Capped Silver Nanoparticles with Positive Surface Charge: Their Catalytic Activity and Antibacterial Spectrum Including Multidrug-Resistant Strains of *Acinetobacter Baumannii*. *Colloids Surf. B* **2017**, *155*, 61-70.
24. Qiao, Z.; Yao, Y.; Song, S.; Yin, M.; Luo, J., Silver Nanoparticles with pH Induced Surface Charge Switchable Properties for Antibacterial and Antibiofilm Applications. *J. Mater. Chem. B* **2019**, *7*, 830-840.
25. Alqahtany, M.; Khadka, P.; Niyonshuti, I.; Krishnamurthi, V. R.; Sadoon, A. A.; Challapalli, S. D.; Chen, J.; Wang, Y., Nanoscale Reorganizations of Histone-Like Nucleoid Structuring Proteins in *Escherichia Coli* Are Caused by Silver Nanoparticles. *Nanotechnology* **2019**, *30*, 385101.
26. Ryu, J. H.; Messersmith, P. B.; Lee, H., Polydopamine Surface Chemistry: A Decade of Discovery. *ACS Appl. Mater. Interfaces* **2018**, *10*, 7523-7540.
27. Liu, Y.; Ai, K.; Lu, L., Polydopamine and Its Derivative Materials: Synthesis and Promising Applications in Energy, Environmental, and Biomedical Fields. *Chem. Rev.* **2014**, *114*, 5057-5115.
28. Liao, Y.; Wang, Y.; Feng, X.; Wang, W.; Xu, F.; Zhang, L., Antibacterial Surfaces through Dopamine Functionalization and Silver Nanoparticle Immobilization. *Mater. Chem. Phys.* **2010**, *121*, 534-540.
29. Sileika, T. S.; Kim, H.-D.; Maniak, P.; Messersmith, P. B., Antibacterial Performance of Polydopamine-Modified Polymer Surfaces Containing Passive and Active Components. *ACS Appl. Mater. Interfaces* **2011**, *3*, 4602-4610.
30. Zhang, Z.; Zhang, J.; Zhang, B.; Tang, J., Mussel-Inspired Functionalization of Graphene for Synthesizing Ag-Polydopamine-Graphene Nanosheets as Antibacterial Materials. *Nanoscale* **2013**, *5*, 118-123.
31. Jiang, J.; Zhu, L.; Zhu, L.; Zhang, H.; Zhu, B.; Xu, Y., Antifouling and Antimicrobial Polymer Membranes Based on Bioinspired Polydopamine and Strong Hydrogen-Bonded Poly(N-vinylpyrrolidone). *ACS Appl. Mater. Interfaces* **2013**, *5*, 12895-12904.
32. Son, H. Y.; Ryu, J. H.; Lee, H.; Nam, Y. S., Silver-Polydopamine Hybrid Coatings of Electrospun Poly(vinyl alcohol) Nanofibers. *Macromol. Mater. Eng.* **2013**, *298*, 547-554.
33. Fu, Y.; Li, G.; Tian, M.; Wang, X.; Zhang, L.; Wang, W., Preparation of Silver Nanoparticle Immobilized Fibrillar Silicate by Poly(dopamine) Surface Functionalization. *J. Appl. Polym. Sci.* **2014**, *131*, 39859.

34. Xie, Y.; Yan, B.; Xu, H.; Chen, J.; Liu, Q.; Deng, Y.; Zeng, H., Highly Regenerable Mussel-Inspired Fe_3O_4@Polydopamine-Ag Core–Shell Microspheres as Catalyst and Adsorbent for Methylene Blue Removal. *ACS Appl. Mate. Interfaces* **2014**, *6*, 8845-8852.
35. Lu, Z.; Xiao, J.; Wang, Y.; Meng, M., *In situ* Synthesis of Silver Nanoparticles Uniformly Distributed on Polydopamine-Coated Silk Fibers for Antibacterial Application. *J. Colloid Interface Sci.* **2015**, *452*, 8-14.
36. Wang, Z.; Ou, J.; Wang, Y.; Xue, M.; Wang, F.; Pan, B.; Li, C.; Li, W., Anti-Bacterial Superhydrophobic Silver on Diverse Substrates Based on the Mussel-Inspired Polydopamine. *Surf. Coat. Technol.* **2015**, *280*, 378-383.
37. Tang, L.; Livi, K. J.; Chen, K. L., Polysulfone Membranes Modified with Bioinspired Polydopamine and Silver Nanoparticles Formed *in situ* to Mitigate Biofouling. *Environ. Sci. Technol. Lett.* **2015**, *2*, 59-65.
38. GhavamiNejad, A.; Aguilar, L. E.; Ambade, R. B.; Lee, S.-H.; Park, C. H.; Kim, C. S., Immobilization of Silver Nanoparticles on Electropolymerized Polydopamine Films for Metal Implant Applications. *Colloids Interface Sci. Commun.* **2015**, *6*, 5-8.
39. Yang, Z.; Wu, Y.; Wang, J.; Cao, B.; Tang, C. Y., *In situ* Reduction of Silver by Polydopamine: A Novel Antimicrobial Modification of a Thin-Film Composite Polyamide Membrane. *Environ. Sci. Technol.* **2016**, *50*, 9543-9550.
40. Yang, E.; Chae, K.-J.; Alayande, A. B.; Kim, K.-Y.; Kim, I. S., Concurrent Performance Improvement and Biofouling Mitigation in Osmotic Microbial Fuel Cells Using a Silver Nanoparticle-Polydopamine Coated Forward Osmosis Membrane. *J. Membr. Sci.* **2016**, *513*, 217-225.
41. Raza, Z. A.; Rehman, A.; Anwar, F.; Usman, A., Development and Antibacterial Performance of Silver Nanoparticles Incorporated Polydopamine–Polyester-Knitted Fabric. *Bull. Mater. Sci.* **2016**, *39*, 391-396.
42. Huang, L.; Zhao, S.; Wang, Z.; Wu, J.; Wang, J.; Wang, S., In Situ Immobilization of Silver Nanoparticles for Improving Permeability, Antifouling and Anti-Bacterial Properties of Ultrafiltration Membrane. *J. Membr. Sci.* **2016**, *499*, 269-281.
43. Jia, Z.; Xiu, P.; Li, M.; Xu, X.; Shi, Y.; Cheng, Y.; Wei, S.; Zheng, Y.; Xi, Y.; Cai, H., et al., Bioinspired Anchoring Agnps onto Micro-Nanoporous TiO_2 Orthopedic Coatings: Trap-Killing of Bacteria, Surface-Regulated Osteoblast Functions and Host Responses. *Biomaterials* **2016**, *75*, 203-222.
44. Cai, R.; Tao, G.; He, H.; Song, K.; Zuo, H.; Jiang, W.; Wang, Y., One-Step Synthesis of Silver Nanoparticles on Polydopamine-Coated Sericin/Polyvinyl Alcohol Composite Films for Potential Antimicrobial Applications. *Molecules* **2017**, *22*, 721.
45. Gao, C.; Wang, Y.; Han, F.; Yuan, Z.; Li, Q.; Shi, C.; Cao, W.; Zhou, P.; Xing, X.; Li, B., Antibacterial Activity and Osseointegration of Silver-Coated Poly(ether ether ketone) Prepared Using the Polydopamine-Assisted Deposition Technique. *J. Mater. Chem. B* **2017**, *5*, 9326-9336.
46. Wu, J.; Yu, C.; Li, Q., Novel Regenerable Antimicrobial Nanocomposite Membranes: Effect of Silver Loading and Valence State. *J. Membr. Sci.* **2017**, *531*, 68-76.
47. Wang, J.; Wu, Y.; Yang, Z.; Guo, H.; Cao, B.; Tang, C. Y., A Novel Gravity-Driven Nanofibrous Membrane for Point-of-Use Water Disinfection: Polydopamine-Induced *in situ* Silver Incorporation. *Sci. Rep.* **2017**, *7*, 1-8.

48. Song, Y.; Jiang, H.; Wang, B.; Kong, Y.; Chen, J., Silver-Incorporated Mussel-Inspired Polydopamine Coatings on Mesoporous Silica as an Efficient Nanocatalyst and Antimicrobial Agent. *ACS Appl. Mater. Interfaces* **2018**, *10*, 1792-1801.
49. Li, Y.; Wang, B.; Sui, X.; Xie, R.; Xu, H.; Zhang, L.; Zhong, Y.; Mao, Z., Durable Flame Retardant and Antibacterial Finishing on Cotton Fabrics with Cyclotriphosphazene/Polydopamine/Silver Nanoparticles Hybrid Coatings. *Appl. Surf. Sci.* **2018**, *435*, 1337-1343.
50. Liu, L.; Cai, R.; Wang, Y.; Tao, G.; Ai, L.; Wang, P.; Yang, M.; Zuo, H.; Zhao, P.; He, H., Polydopamine-Assisted Silver Nanoparticle Self-Assembly on Sericin/Agar Film for Potential Wound Dressing Application. *Int. J. Mol. Sci.* **2018**, *19*, 2875.
51. Yang, E.; Alayande, A. B.; Kim, C.-M.; Song, J.-H.; Kim, I. S., Laminar Reduced Graphene Oxide Membrane Modified with Silver Nanoparticle-Polydopamine for Water/Ion Separation and Biofouling Resistance Enhancement. *Desalination* **2018**, *426*, 21-31.
52. Cordes, A. L.; Merkel, D. R.; Patel, V. J.; Courtney, C.; McBride, M.; Yakacki, C. M.; Frick, C. P., Mechanical Characterization of Polydopamine-Assisted Silver Deposition on Thiol-ene Polymer Substrates. *Surf. Coat. Technol.* **2019**, *358*, 136-143.
53. Guan, M.; Chen, Y.; Wei, Y.; Song, H.; Gao, C.; Cheng, H.; Li, Y.; Huo, K.; Fu, J.; Xiong, W., Long-Lasting Bactericidal Activity through Selective Physical Puncture and Controlled Ions Release of Polydopamine and Silver Nanoparticles–Loaded TiO_2 Nanorods *in vitro* and *in vivo*. *Int. J. Nanomedicine* **2019**, *14*, 2903.
54. Shang, B.; Xu, M.; Zhi, Z.; Xi, Y.; Wang, Y.; Peng, B.; Li, P.; Deng, Z., Synthesis of Sandwich-Structured Silver@Polydopamine@Silver Shells with Enhanced Antibacterial Activities. *J. Colloid Interface Sci.* **2020**, *558*, 47-54.
55. Orishchin, N.; Crane, C. C.; Brownell, M.; Wang, T.; Jenkins, S.; Zou, M.; Nair, A.; Chen, J., Rapid Deposition of Uniform Polydopamine Coatings on Nanoparticle Surfaces with Controllable Thickness. *Langmuir* **2017**, *33*, 6046-6053.
56. Krishnamurthi, V. R.; Niyonshuti, I.; Chen, J.; Wang, Y., A New Method Based on Time Derivatives of Optical Density and/or Fluorescence for Evaluating Bacterial Growth with Microplate Readers. **2020**, Under review.
57. Zhang, Q.; Li, W.; Wen, L. P.; Chen, J.; Xia, Y., Facile Synthesis of Ag Nanocubes of 30 to 70 nm in Edge Length with CF_3COOAg as a Precursor. *Chem. Eur. J.* **2010**, *16*, 10234-10239.
58. Brewster, J. D., A Simple Micro-Growth Assay for Enumerating Bacteria. *J. Microbiol. Methods* **2003**, *53*, 77-86.
59. Haque, M. A.; Imamura, R.; Brown, G. A.; Krishnamurthi, V. R.; Niyonshuti, I. I.; Marcelle, T.; Mathurin, L. E.; Chen, J.; Wang, Y., An Experiment-Based Model Quantifying Antimicrobial Activity of Silver Nanoparticles on *Escherichia Coli*. *RSC Adv.* **2017**, *7*, 56173-56182.
60. Schneider, C. A.; Rasband, W. S.; Eliceiri, K. W., NIH Image to ImageJ: 25 Years of Image Analysis. *Nat. Methods* **2012**, *9*, 671-675.
61. Schindelin, J.; Arganda-Carreras, I.; Frise, E.; Kaynig, V.; Longair, M.; Pietzsch, T.; Preibisch, S.; Rueden, C.; Saalfeld, S.; Schmid, B., Fiji: An Open-Source Platform for Biological-Image Analysis. *Nat. Methods* **2012**, *9*, 676-682.
62. Rasband, W. S., ImageJ. Bethesda, MD: 1997.
63. Stevenson, K.; McVey, A. F.; Clark, I. B.; Swain, P. S.; Pilizota, T., General Calibration of Microbial Growth in Microplate Readers. *Sci. Rep.* **2016**, *6*, 1-7.

64. Lemire, J. A.; Kalan, L.; Bradu, A.; Turner, R. J., Silver Oxynitrate, an Unexplored Silver Compound with Antimicrobial and Antibiofilm Activity. *Antimicrob. Agents Chemother.* **2015**, *59*, 4031-4039.
65. Schweigert, N.; Zehnder, A. J. B.; Eggen, R. I. L., Chemical Properties of Catechols and Their Molecular Modes of Toxic Action in Cells, from Microorganisms to Mammals. *Environ. Microbiol.* **2001**, *3*, 81-91.
66. Beamson, G.; Briggs, D., *High Resolution XPS of Organic Polymers: The Scienta ESCA300 Database*; Wiley, 1992.
67. An, T.; Lee, N.; Cho, H.-J.; Kim, S.; Shin, D.-S.; Lee, S.-M., Ultra-Selective Detection of Fe^{2+} Ion by Redox Mechanism Based on Fluorescent Polymerized Dopamine Derivatives. *RSC adv.* **2017**, *7*, 30582-30587.
68. Silverstein, R. M.; Webster, F. X.; Kiemle, D., *Spectrometric Identification of Organic Compounds, 7th Edition*; Wiley, 2005.
69. Talbi, H.; Maarouf, E. B.; Humbert, B.; Alnot, M.; Ehrhardt, J. J.; Ghanbaja, J.; Billaud, D., Spectroscopic Studies of Electrochemically Doped Polyindole. *J. Phys. Chem. Solids* **1996**, *57*, 1145-1151.
70. Okuda, H.; Wakamatsu, K.; Ito, S.; Sota, T., Possible Oxidative Polymerization Mechanism of 5,6-Dihydroxyindole from Ab Initio Calculations. *J. Phys. Chem. A* **2008**, *112*, 11213-11222.
71. Stark, G., Functional Consequences of Oxidative Membrane Damage. *J. Membr biol.* **2005**, *205*, 1-16.
72. Su, L.; Yu, Y.; Zhao, Y.; Liang, F.; Zhang, X., Strong Antibacterial Polydopamine Coatings Prepared by a Shaking-Assisted Method. *Sci.Rep.* **2016**, *6*, 24420.
73. Forooshani, K. P.; Polega, E.; Thomson, K.; Bhuiyan, M. S. A.; Pinnaratip, R.; Trought, M.; Kendrick, C.; Gao, Y.; Perrine, K. A.; Pan, L., et al., Antibacterial Properties of Mussel-Inspired Polydopamine Coatings Prepared by a Simple Two-Step Shaking-Assisted Method. *Front. Chem.* **2019**, *7*, 631.

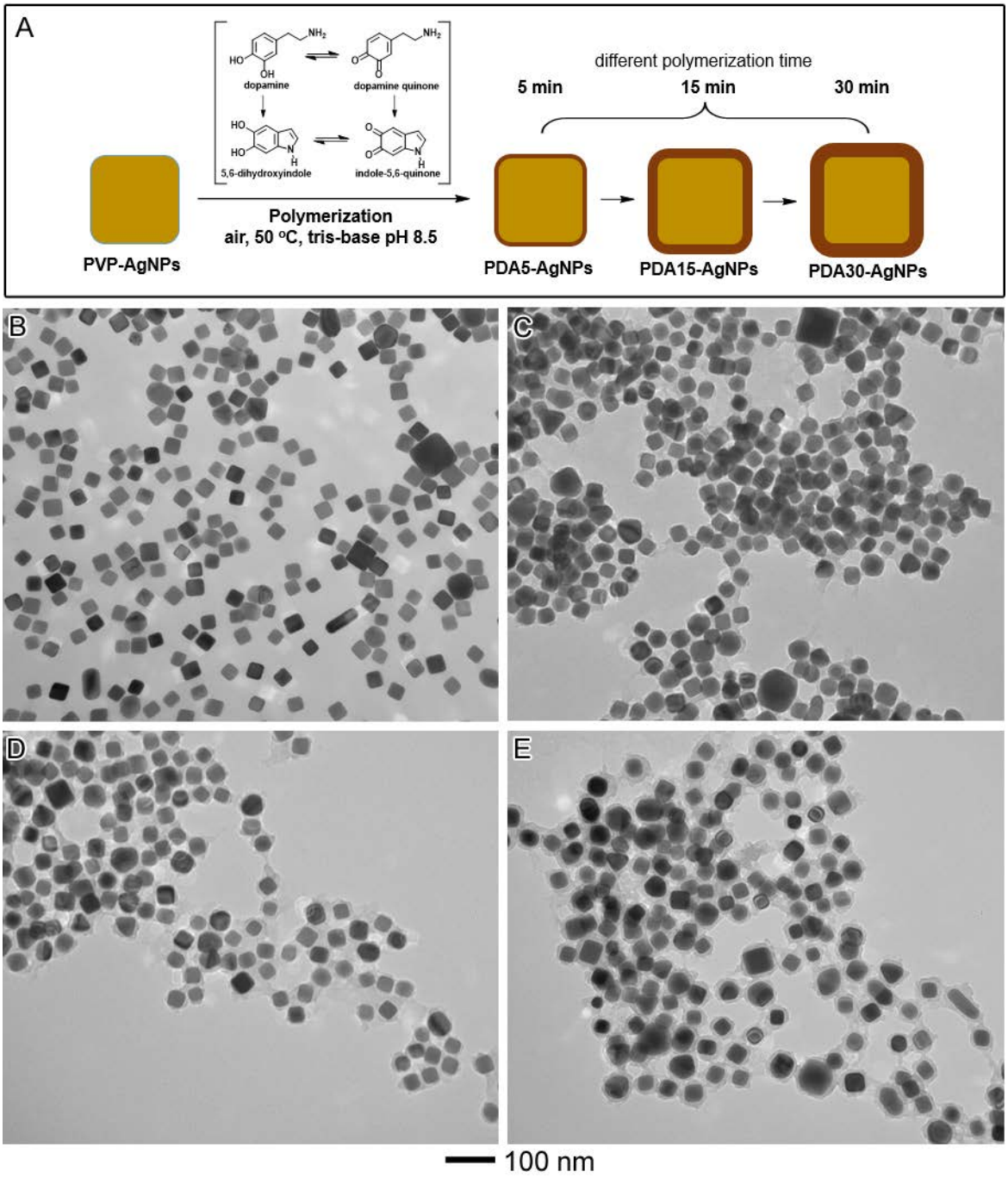

Figure 1. (A) Schematic illustration of the PDA deposition on PVP-AgNPs to form PDA-AgNPs at different time points. (B-E) TEM characterization of AgNPs: (B) PVP-AgNPs; (C-E) PDA-AgNPs obtained at different lengths of PDA coating time, 5, 15, and 30 min, respectively, denoted as PDA5-AgNPs (C), PDA15-AgNPs (D), and PDA30-AgNPs (E).

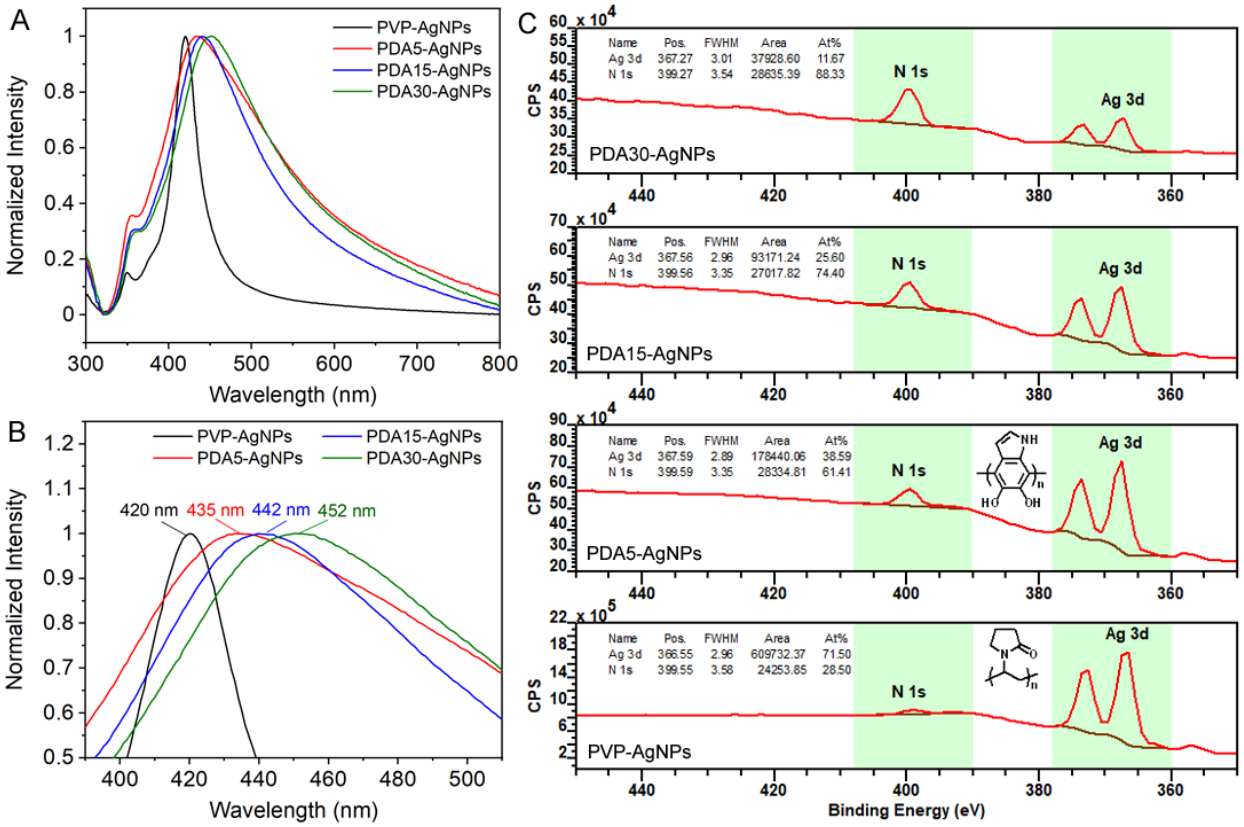

Figure 2. (A) UV-vis spectra of AgNPs before and after PDA coating process: PVP-AgNPs (black), PDA5-AgNPs (red), PDA15-AgNPs (blue), and PDA30-AgNPs (green); (B) Zoom-in view of the spectra in (A) to identify the peak positions of each samples; (C) XPS spectra of Ag 3d and N 1s for the corresponding dry samples in (A). The baseline was corrected by the Shirley and linear method for Ag 3d and N 1s, respectively. The insets are the repeating units of PVP and PDA illustrating that each repeating unit contains one N atom.

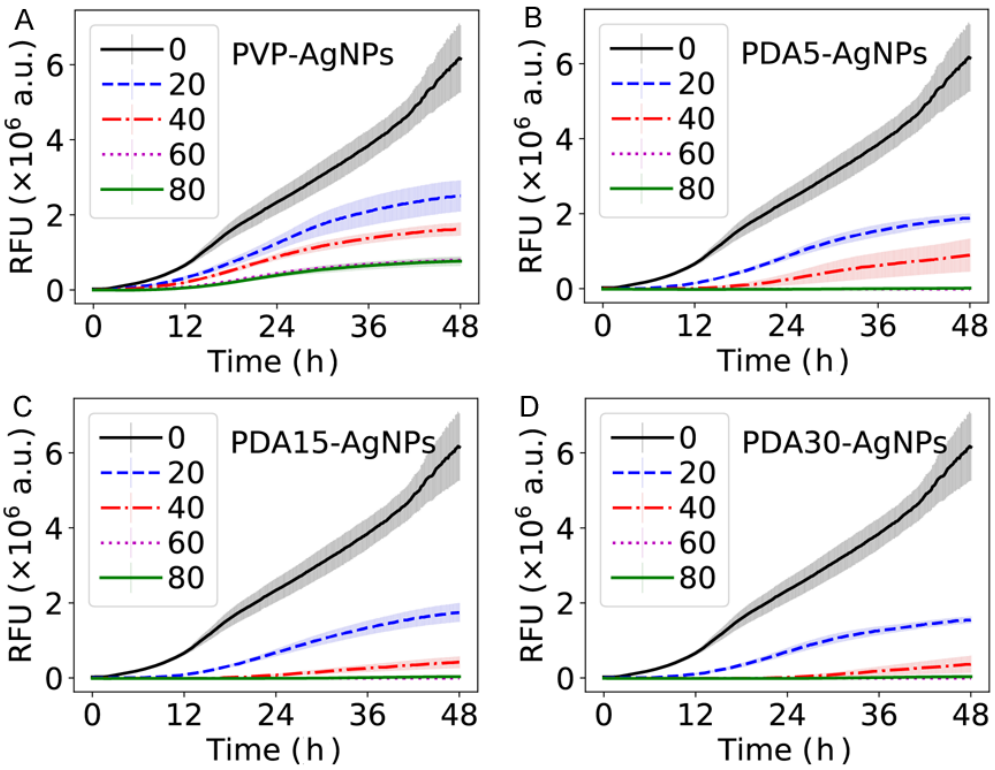

Figure 3. Fluorescence-based growth curves of AgNPs with different coatings: (A) PVP-AgNPs; (B) PDA5-AgNPs; (C) PDA15-AgNPs; and (D) PDA30-AgNPs. The fluorescence intensities of bacterial culture in microplate wells as functions of time at various concentrations of 0 (untreated – negative control; black solid line), 20 (blue dashed lines), 40 (red dot-dashed lines), 60 (magenta dotted lines), and 80 (green solid lines) μg/mL. The lines indicate the means of at least four replicates. Error bars (lighter areas) represent the standard errors of the means.

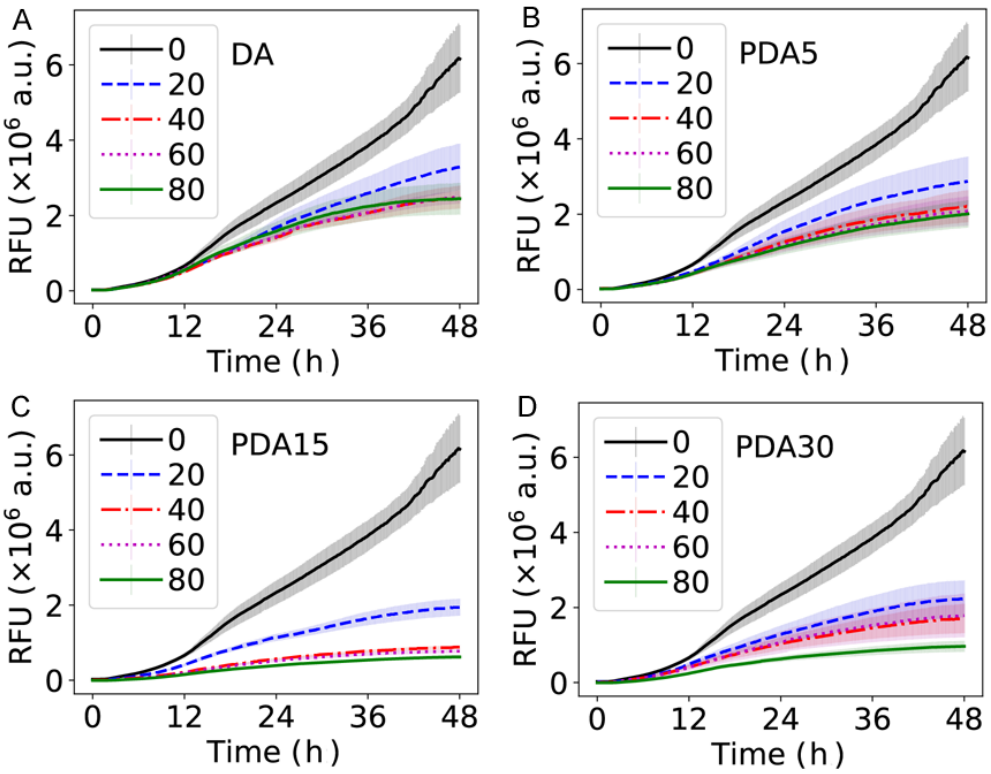

Figure 4. Fluorescence-based growth curves of PDA synthesized at the same conditions as the coating process but in the absence of AgNPs: (A) 0 min (DA monomer); (B) 5 min (PDA5); (C) 15 min (PDA15); and (D) 30 min (PDA30). The fluorescence intensities of bacterial culture in microplate wells as functions of time at various concentrations of 0 (untreated – negative control; black solid line), 20 (blue dashed lines), 40 (red dot-dashed lines), 60 (magenta dotted lines), and 80 (green solid lines) μg/mL. The lines indicate the means of at least four replicates. Error bars (lighter areas) represent the standard errors of the means.

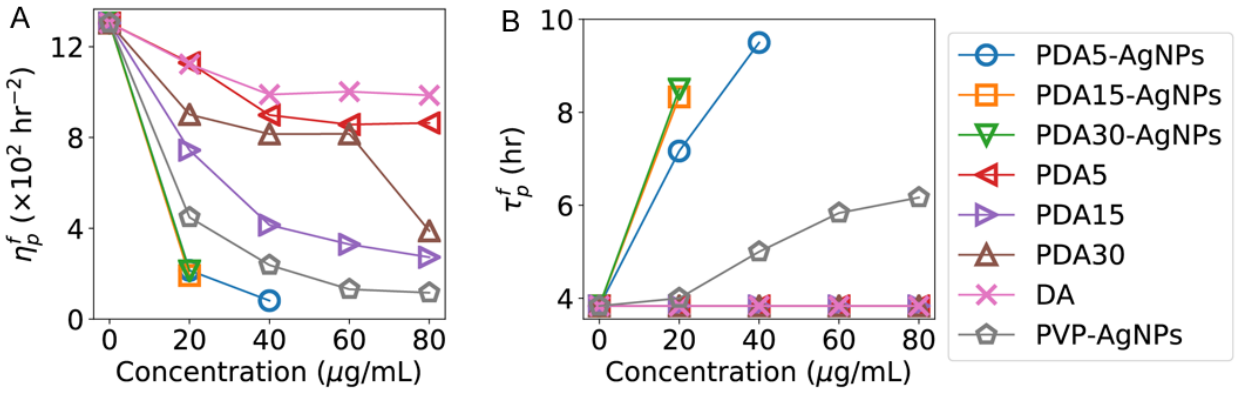

Figure 5. Dependence of the heights (A, η_p^f) and locations (B, τ_p^f) of the peaks, observed in the second-order time derivatives of the fluorescence growth curves, on the concentration of PDA, PDA-AgNPs, DA, and PVP-AgNPs.

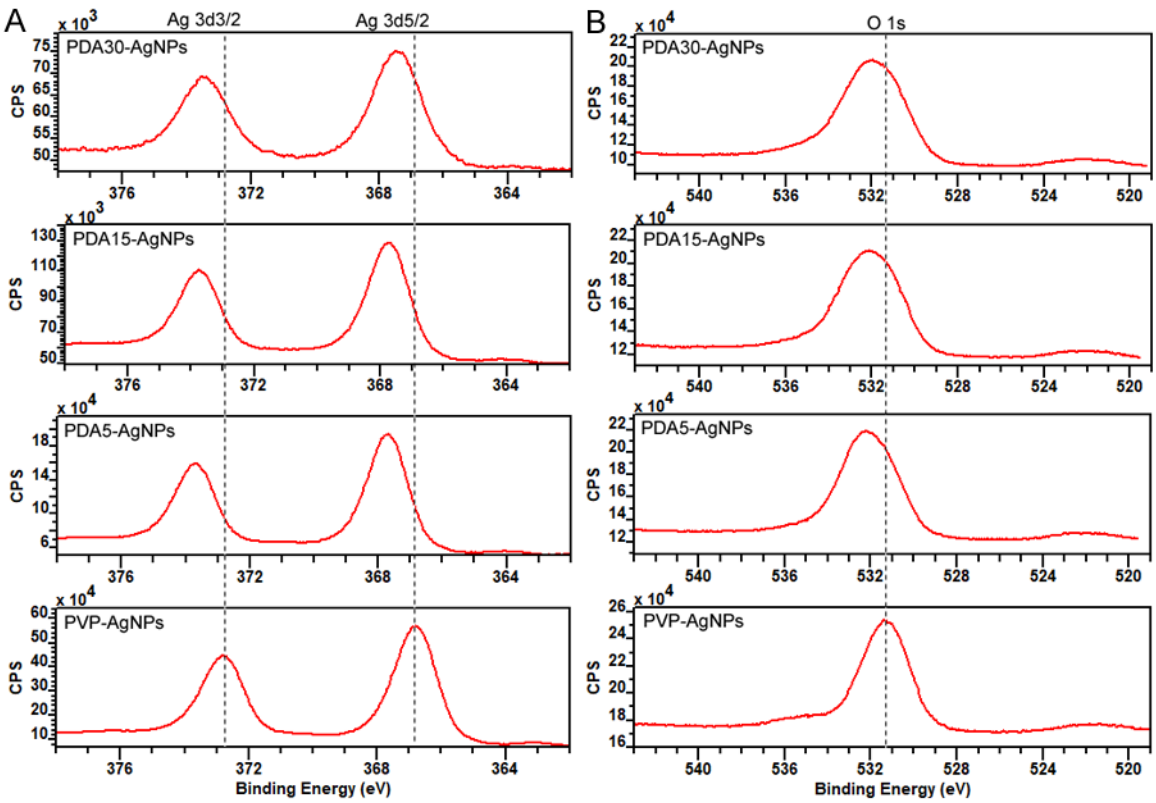

Figure 6. XPS of Ag 3d (A) and O 1s (B). Samples from bottom to top are corresponding to PVP-AgNPs, PDA5-AgNPs, PDA15-AgNPs, and PDA30-AgNPs.

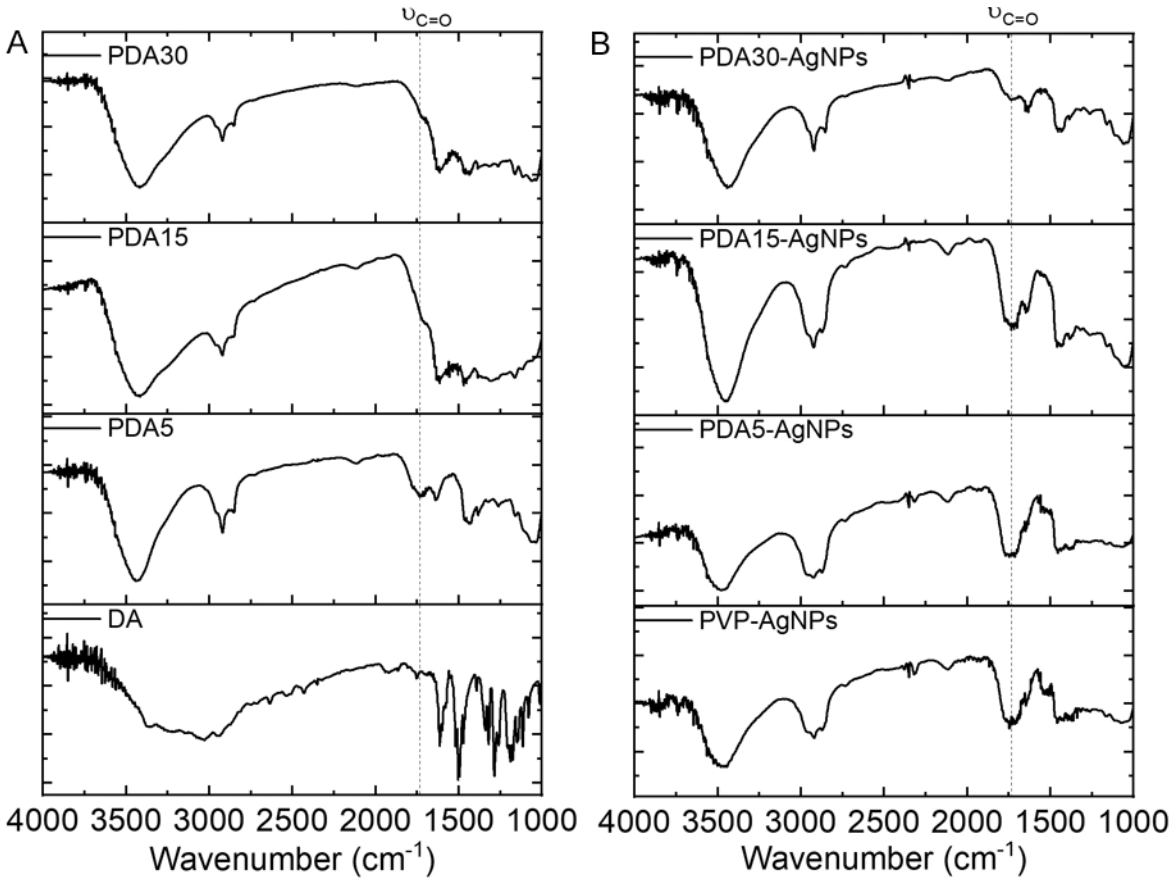

Figure 7. FTIR spectra of samples without or with AgNPs: (A) from bottom to top corresponding to DA, PDA5, PDA15, and PDA30; and (B) from bottom to top corresponding to PVP-AgNPs, PDA5-AgNPs, PDA15-AgNPs, and PDA30-AgNPs.

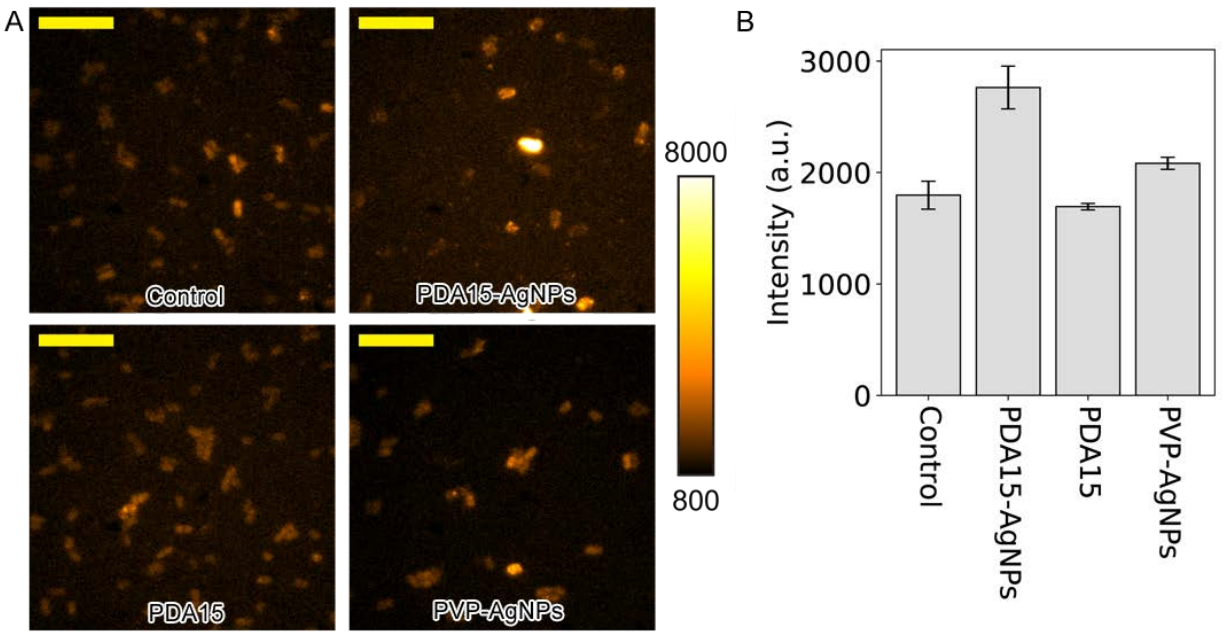

Figure 8. Promoted generation of ROS by PDA-AgNPs. (A) Representative fluorescent images of bacteria stained by CellROX® Orange Reagent. Scale bar = 10 μm. (B) Mean fluorescence intensities of the stained bacteria. Error bars represent the standard error of the mean.

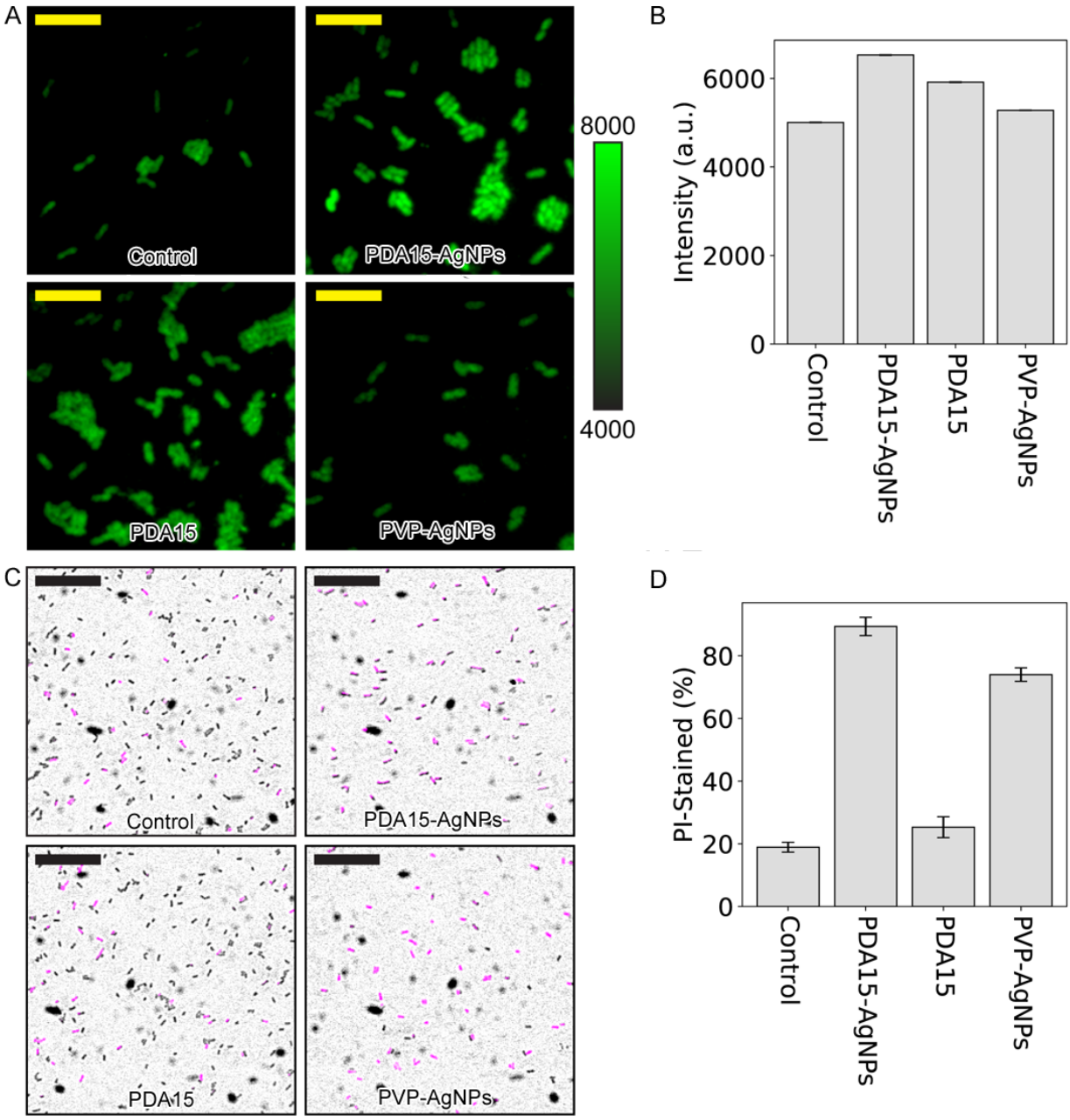

Figure 9. Higher membrane damage caused by PDA-AgNPs. (A) Representative fluorescent images of bacteria stained by MitoTracker Green FM dye. Scale bar = 10 μm. (B) Mean fluorescence intensities of the Mito-Tracker stained bacteria. Error bars represent the standard error of the mean. (C) Representative fluorescent images of bacteria stained by PI (purple) on top of the corresponding phase contrast images (grayscale). Scale bar = 25 μm. (D) Mean percentage of the PI-stained bacteria. Error bars represent the standard error of the mean.

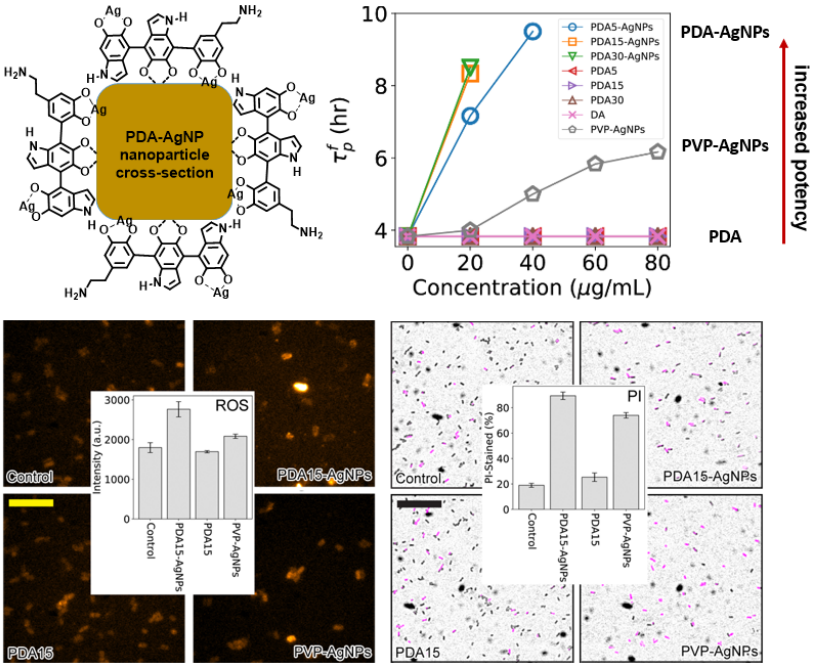
PDA-AgNP nanoparticle cross-section
PDA5-AgNPs
PDA15-AgNPs
PDA30-AgNPs
PDA5
PDA15
PDA30
DA
PVP-AgNPs
PDA-AgNPs
PVP-AgNPs
PDA
increased potency
Concentration (μg/mL)
ROS
Intensity (a.u.)
Control
PDA15-AgNPs
PDA15
PVP-AgNPs
PI
PI-Stained (%)

TOC

Supporting Information

Polydopamine Surface Coating Synergizes Antimicrobial Activity of Silver Nanoparticles

Isabelle I. Niyonshuti,[1,†] Venkata Rao Krishnamurthi,[2,†] Deborah Okyere,[3] Liang Song,[1] Mourad Benamara,[4] Xiao Tong,[5] Yong Wang,[2,3,6,*] Jingyi Chen[1,3,*]

[1]Department of Chemistry and Biochemistry, University of Arkansas, Fayetteville, AR 72701, USA

[2]Department of Physics, University of Arkansas, Fayetteville, AR 72701, USA

[3]Microelectronics-Photonics Graduate Program, University of Arkansas, Fayetteville, AR 72701, USA

[4]Institute of Nanoscience and Engineering, University of Arkansas, Fayetteville, AR 72701, USA

[5]Center for Functional Nanomaterials, Brookhaven National Laboratory, Upton, NY 11973, USA

[6]Cell and Molecular Biology Graduate Program, University of Arkansas, Fayetteville, AR 72701, USA

[†]These authors contributed to this work equally.

*Corresponding authors: chenj@uark.edu (nanoparticles); yongwang@uark.edu (antimicrobials)

Table S1. Hydrodynamic diameter and zeta potential measurements of surface-modified AgNPs.

Surface-modified AgNPs	Hydrodynamic diameter (nm) in water	Zeta potential (mV) in PBS pH = 7.4
PVP-AgNPs	121.7±4.0	-8.74±1.08
PDA5-AgNPs	119.6±2.4	-14.70±2.67
PDA15-AgNPs	186.3±2.0	-10.26±0.89
PDA30-AgNPs	209.3±4.7	-9.52±0.22
DA-AgNPs	113.1±1.9	-12.14±1.97

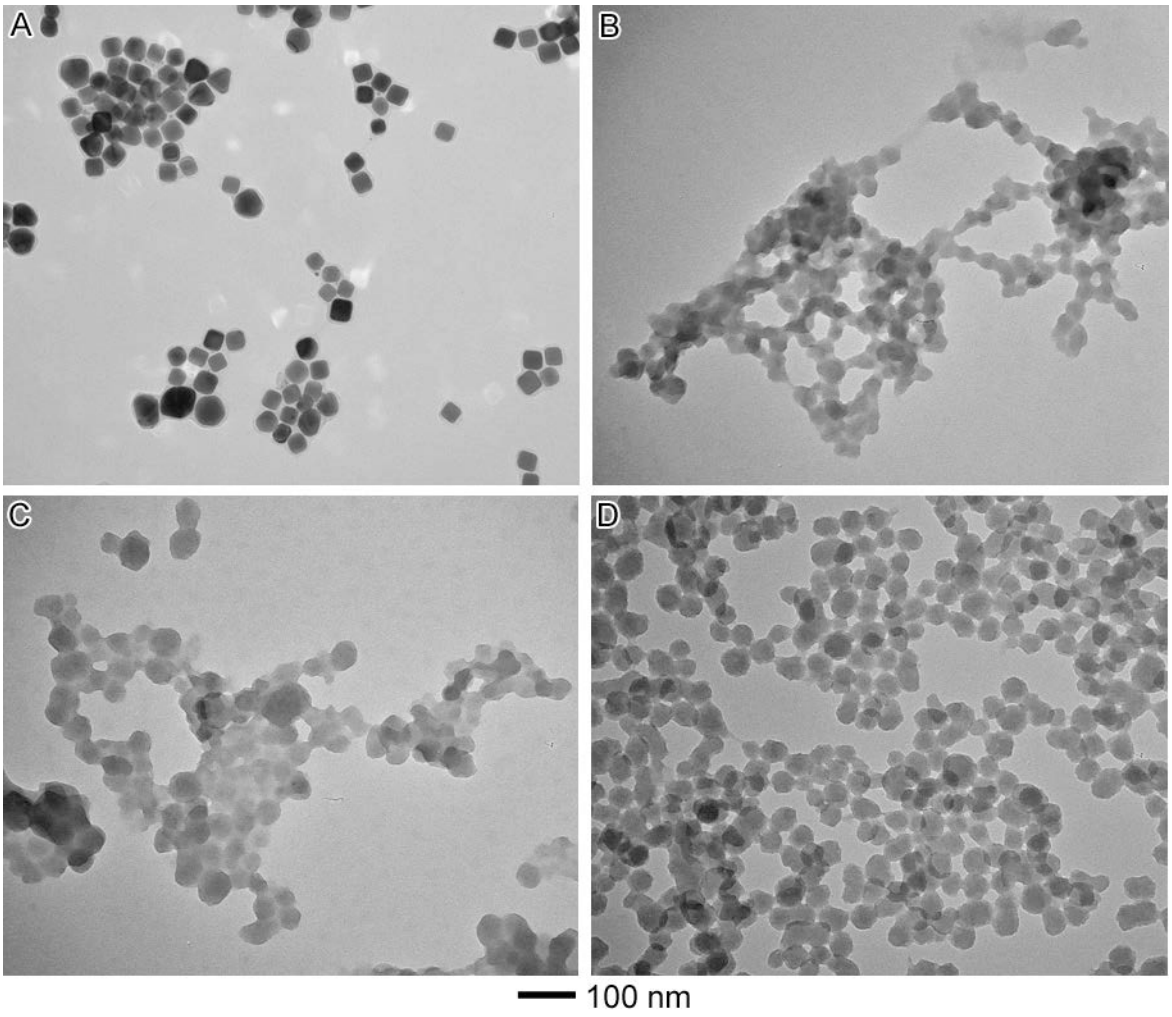

Figure S1. TEM characterization of DA-AgNPs (A) and PDA obtained at different reaction time periods, 5, 15, and 30 min, respectively, denoted as PDA5 (B), PDA (C), and PDA30 (D).

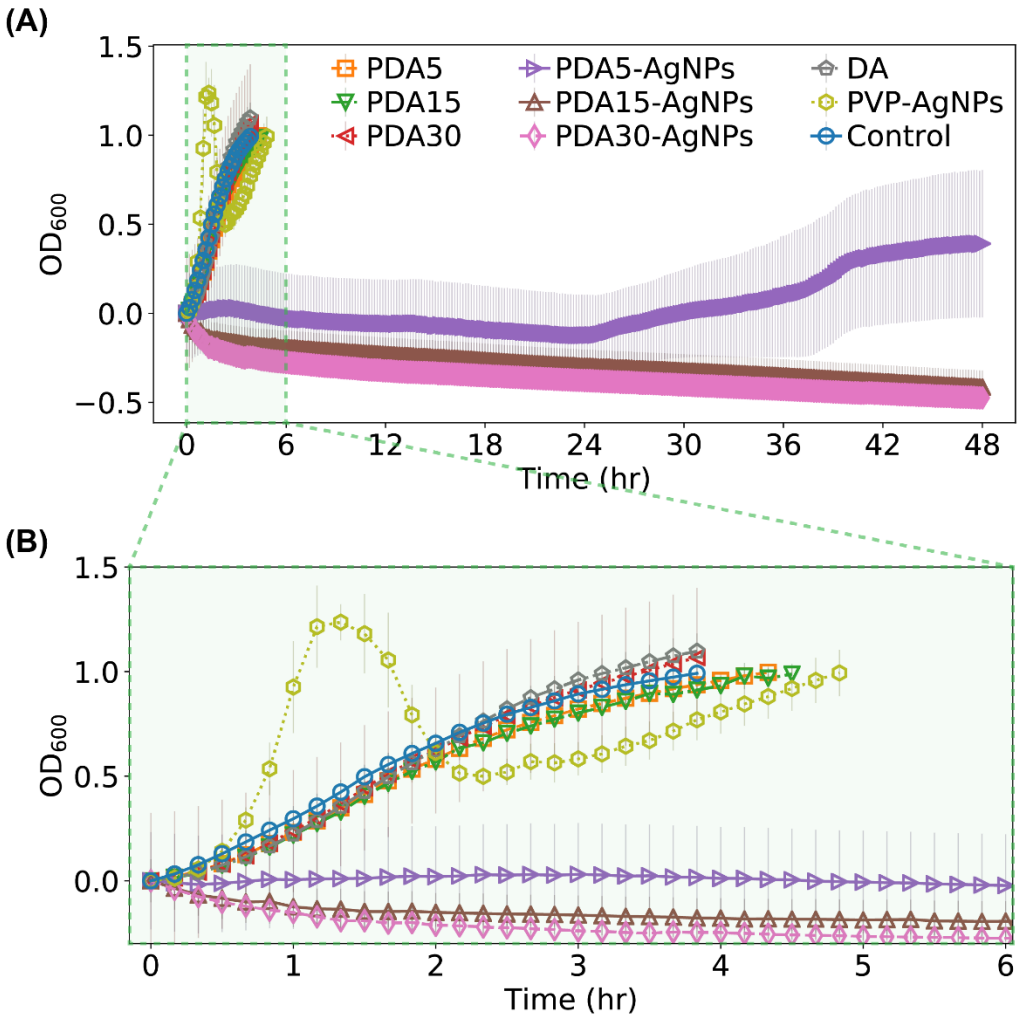

Figure S2. Truncated and vertically shifted OD growth curves for bacteria treated with PDA, PDA-AgNPs, DA and PVP-AgNPs: (A) full region of 48 h incubation; and (B) zoom-in region of 0-6 h incubation.

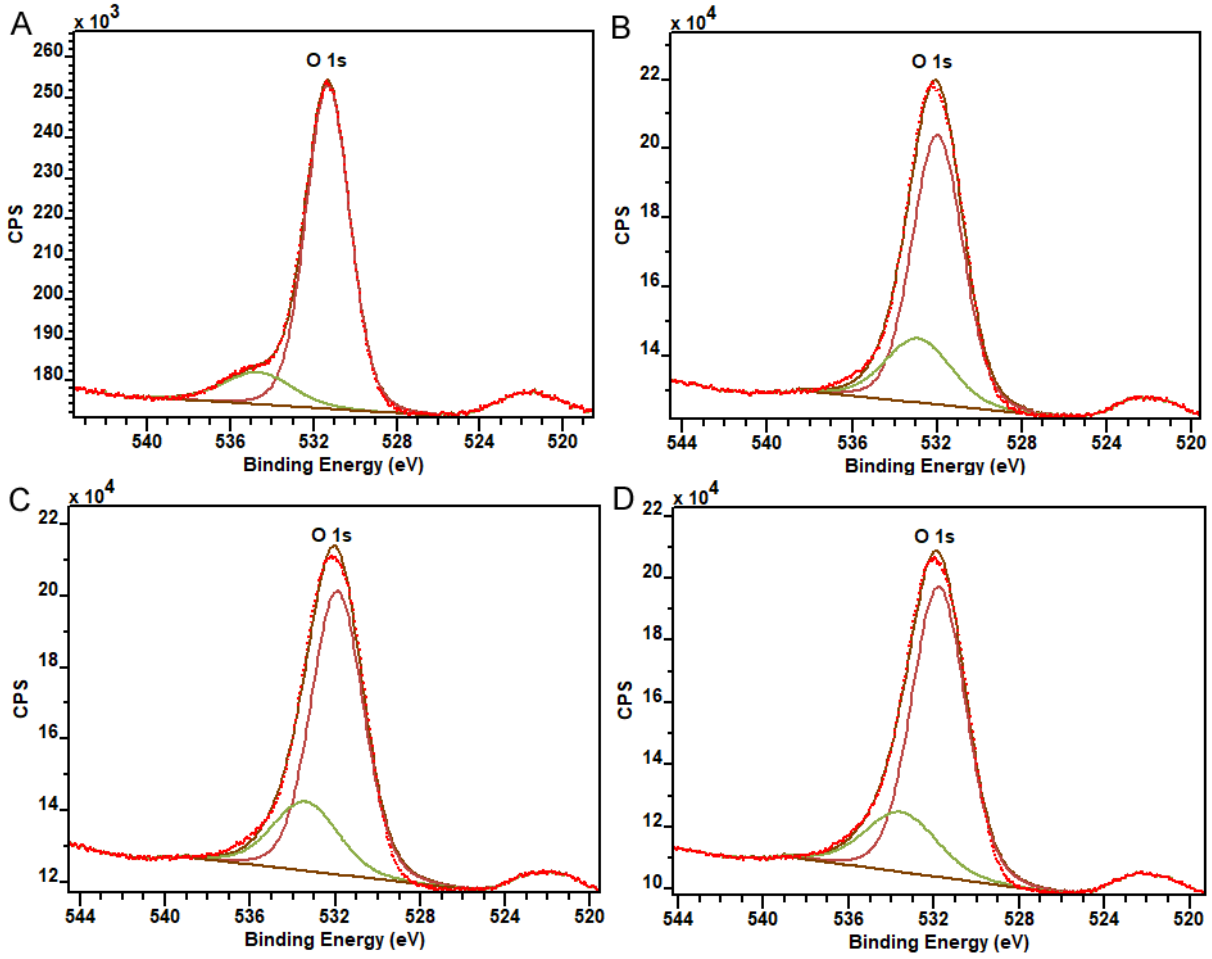

Figure S3. XPS deconvoluted spectra of O 1s for different samples: (A) PVP-AgNPs; (B) PDA5-AgNPs; (C) PDA15-AgNPs; and (D) PDA30-AgNPs. The dotted lines (red) are the experimental data while the solid lines (dark brown) are the fitting sum after the linear background subtraction. The solid lines in light brown and light green are the fitting C=O and C-OH components, respectively. For PVP, the C=O and C-OH are attached to a N corresponding to N-C=O and N-C-OH while the C=O and C-OH are on aromatic rings of PDA.

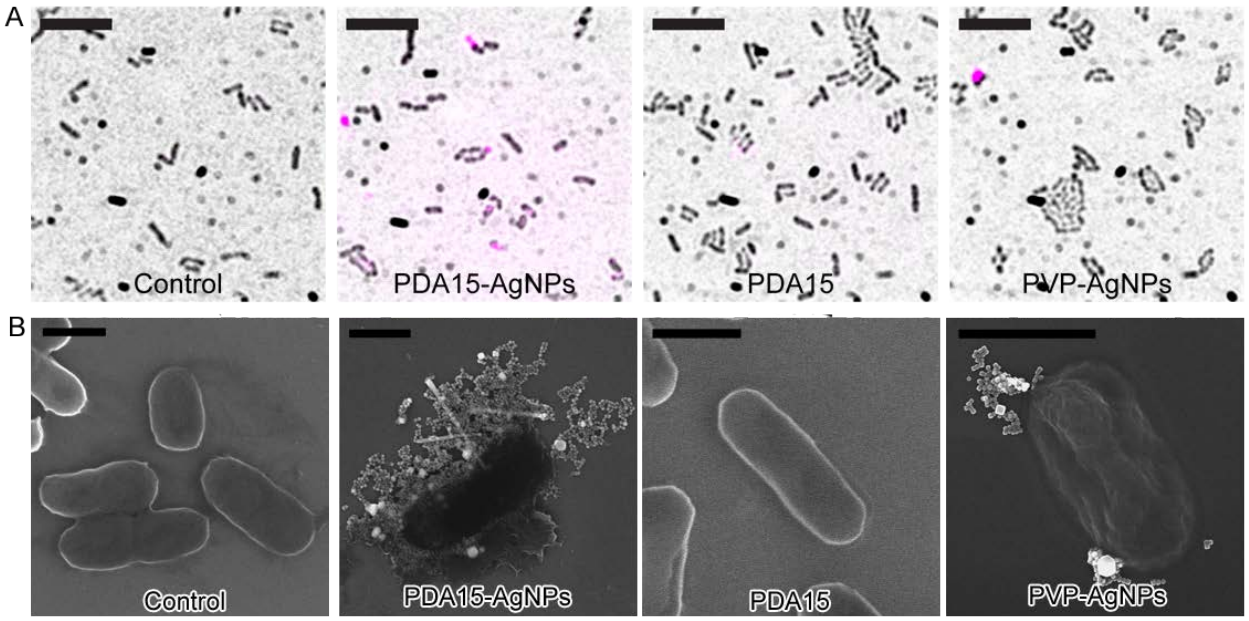

Figure S4. (A) Representative fluorescent images of nanoparticles (purple) on top of the bright images of bacteria (grayscale) treated with different conditions. Scale bar = 10 μm. (B) Representative SEM images of the bacteria treated with different conditions. Scale bar = 1 μm.